Inorganic Chemistry

Article

pubs.acs.org/IC

Solution Structures, Stabilities, Kinetics, and Dynamics of DO3A and DO3A–Sulphonamide Complexes

Anett Takács,[†] Roberta Napolitano,[⊥] Mihály Purgel,[‡] Attila Csaba Bényei,[§] László Zékány,[†] Ernő Brücher,[†] Imre Tóth,[†] Zsolt Baranyai,*[,†] and Silvio Aime*[,∥]

[†]Department of Inorganic and Analytical Chemistry, [‡]MTA-DE Homogeneous Catalysis and Reaction Mechanisms Research Group, [§]Department of Physical Chemistry, University of Debrecen, H-4032 Debrecen, Egyetem tér 1, Hungary

[⊥]Centro Ricerche Bracco, Bracco Imaging Spa, Via Ribes 5, I-10010 Colleretto Giacosa, Italy

[∥]Department of Molecular Biotechnology and Health Sciences, Molecular Imaging Center, University of Torino, Via Nizza 52, 10126 Torino, Italy

Supporting Information

ABSTRACT: The Gd^{3+}-DO3A–arylsulphonamide (DO3A–SA) complex is a promising pH-sensitive MRI agent. The stability constants of the DO3A–SA and DO3A complexes formed with Mg^{2+}, Ca^{2+}, Mn^{2+}, Zn^{2+}, and Cu^{2+} ions are similar, whereas the $\log K_{LnL}$ values of Ln(DO3A–SA) complexes are 2 orders of magnitude higher than those of the Ln(DO3A) complexes. The protonation constant ($\log K_{MHL}$) of the sulphonamide nitrogen in the Mg^{2+}, Ca^{2+}, Mn^{2+}, Zn^{2+}, and Cu^{2+} complexes is very similar to that of the free ligand, whereas the $\log K_{LnHL}$ values of the Ln(DO3A–SA) complexes are lower by about 4 $\log K$ units, indicating a strong interaction between the Ln^{3+} ions and the sulphonamide N atom. The Ln(HDO3A–SA) complexes are formed via triprotonated *Ln(H_3DO3A–SA) intermediates which rearrange to the final complex in an OH^--assisted deprotonation process. The transmetalation reaction of Gd(HDO3A–SA) with Cu^{2+} is very slow ($t_{1/2} = 5.6 \times 10^3$ h at pH = 7.4), and it mainly occurs through proton-assisted dissociation of the complex. The ^1H and ^{13}C NMR spectra of the La-, Eu-, Y-, and Lu(DO3A–SA) complexes have been assigned using 2D correlation spectroscopy (COSY, EXSY, HSQC). Two sets of signals are observed for Eu-, Y-, and Lu(DO3A–SA), showing two coordination isomers in solution, that is, square antiprismatic (SAP) and twisted square antiprismatic (TSAP) geometries with ratios of 86–14, 93– 7, and 94–6%, respectively. Line shape analysis of the ^{13}C NMR spectra of La-, Y- , and Lu(DO3A–SA) gives higher rates and lower activation entropy values compared to Ln(DOTA) for the arm rotation, which indicates that the Ln(DO3A–SA) complexes are less rigid due to the larger flexibility of the ethylene group in the sulphonamide pendant arm. The fast isomerization and the lower activation parameters of Ln(DO3A–SA) have been confirmed by theoretical calculations in vacuo and by using the polarizable continuum model. The solid state X-ray structure of Cu(H_2DO3A–SA) shows distorted octahedral coordination. The coordination sites of Cu^{2+} are occupied by two ring N- and two carboxylate O-atoms in equatorial position. The other two ring N-atoms complete the coordination sphere in axial positions. The solid state structure also indicates that a carboxylate O atom and the sulphonamide nitrogen are protonated and noncoordinated.

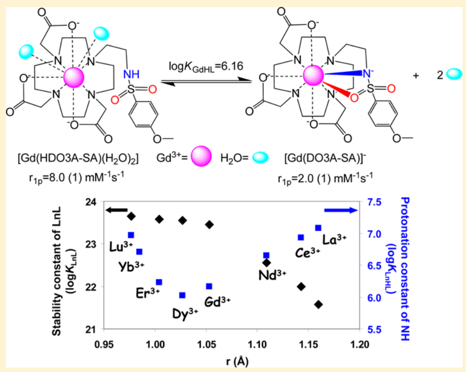

■ INTRODUCTION

Since the introduction of the open-chain Gd(DTPA) and macrocyclic Gd(DOTA) complexes as nonspecific, extracellular contrast agents (CAs) in MRI examinations in 1988, several similar, as well as tissue specific (liver imaging and blood pool) agents were developed and approved for clinical use.[1,2] In recent years, considerable efforts are made to develop contrast agents for the detection of changes in pH, pO_2, metal ions, small molecules, and enzyme concentrations in tissues by "responsive" or "smart" contrast agents.[3−5] The detection of pH changes in principle can localize tumor tissues, sites of inflammation, and infection where the pH is lower (5.5–7.0) than the physiological pH.[3,4,6−10]

The contrast-enhancing effect of Gd^{3+} complexes is based on the increase of proton relaxation rates ($R_1 = 1/T_1$, where T_1 is the longitudinal relaxation time) in tissues in the vicinity of contrast agents. The relaxation effect of contrast agents is expressed by the relaxivity, that is, the increase in the water proton relaxation rates per unit concentration of contrast agent (r_1, mM^{-1} s^{-1}). In all the commercial contrast agents, Gd^{3+} is coordinated by an octadentate aminopolycarboxylate ligand, and the ninth coordination site of Gd^{3+} is occupied by a water molecule. This water exchanges rapidly with the surrounding water molecules and transfers the paramagnetic effect of Gd^{3+}

Received: October 14, 2013
Published: February 24, 2014

to the bulk water. In the responsive contrast agents, a heptadentate ligand is quite often coordinated to the Gd^{3+}, and there are two water molecules directly bound to the metal center.[3,4,11−13] The relaxation effect of Gd^{3+} complexes increases with the number of water molecules, directly bound to the Gd^{3+} (q), and therefore the relaxivity of these complexes is higher. One or both directly bound water molecules can be replaced by the donor atom(s) of another ligand or an intramolecular appended group, causing a drop of relaxivity. If the replacement of the water molecule(s) is pH-dependent and occurs in the pH range of 5−8, then the system in principle is suitable to detect pH changes under biological conditions.[3,4,11−13]

In pH-responsive contrast agents, the heptadentate ligands are generally based on the macrocyclic DO3A (Scheme 1),

Scheme 1. Structure of H_4DO3A−SA, H_3DO3A, and H_4DOTA Ligands Discussed in This Work

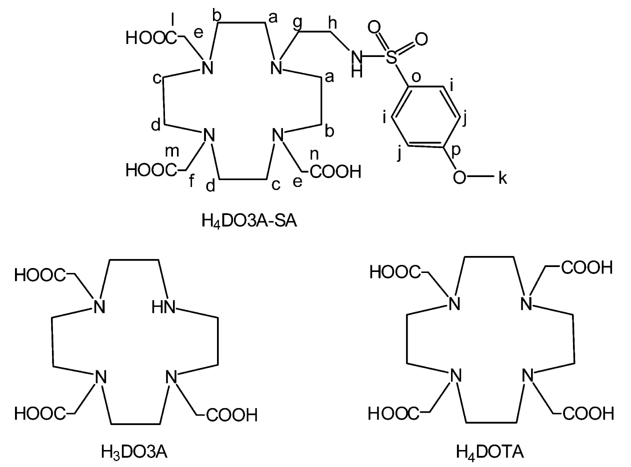

because the complexes formed with its derivatives are sufficiently stable and inert for biological use.[5,14] In the search for a suitable functional group, the behavior of the arylsulphonamide group seemed to be promising as a potential candidate. The coordination of the deprotonated sulphonamide nitrogen to Zn^{2+} was found to be pH-dependent.[15] Lowe et al. synthesized several DO3A derivative ligands in which the deprotonation and coordination of the β-arylsulphonamide nitrogen was pH-dependent.[16] By varying the *para*-substituents in the arylsulphonamide moiety, the pH range of deprotonation of the sulphonamide group could be modified. The pH dependence of the relaxivity values of the Gd^{3+} complexes and that of the luminescence behavior of the Eu^{3+} and Tb^{3+} complexes indicated that the HDO3A−SA^{3-} could be coordinated as a heptadentate ligand at lower pH values (the sulphonamide group was not coordinated, therefore $q = 2$). At higher pH values, the H^+ might dissociate from the −NH−SO_2− group, and the DO3A−SA^{4-} behaved like an octadentate ligand.[11] The relaxation and luminescence properties of complexes formed with the β-carboxyalkyl-containing ligands did not alter in the presence of endogenous ligands or serum albumin, indicating the promising behavior of the complexes.[11] However, the concentration of Gd^{3+}-DO3A−sulphonamide complexes should be known for the measurement of pH in tissues. More recently, Gianolio et al. proposed to use the "guest" molecule adamantine, which was labeled either with Gd(DO3A−SA) or with CF_3 for the interaction with the poly-β-cyclodextrin "host" molecule, when the Gd/^{19}F ratiometric method could be used to determine the concentration of the Gd^{3+} complex in the adduct.[17] Frullano et al. proposed a dual MRI/PET pH-responsive agent with the use of the pH-sensitive Gd(DOTA-4AmP), which was labeled by ^{18}F isotope for the determination of the chemical concentration of the complex by PET experiments.[18] With the use of similar approach, a dual MRI/SPECT pH-responsive agent was developed by the use of Gd(DO3A−SA) and ^{166}Ho-labeled Ho(DO3A−SA), where the ^{166}Ho complex acts as a concentration reporter.[19] These efforts clearly indicate the potential significance of Gd(DO3A−SA) and its derivative complexes. In order to use the complexes in clinical practice, the complexation behavior of the DO3A−sulphonamide ligand and the properties of its complexes with Gd^{3+}, other lanthanides and also with the most important endogenous metal ions (Mg^{2+}, Ca^{2+}, Zn^{2+}, and Cu^{2+}) should be known. The sulphonamide moiety is used quite rarely as a ligating group, although the negatively charged amide N^- atom is a very interesting and peculiar donor atom, particularly for the complexation of lanthanides. Thus, the study of the complexes of the DO3A−SA, the equilibrium, the kinetics, and structural properties are fascinating also for the coordination chemistry of lanthanides.

■ EXPERIMENTAL SECTION

Materials. The chemicals used for the experiments were of the highest analytical grade. The concentration of $MgCl_2$, $CaCl_2$, $MnCl_2$, $ZnCl_2$, $CuCl_2$, and $LnCl_3$ solutions were determined by complexometric titration with standardized Na_2H_2EDTA and xylenol orange ($ZnCl_2$, and $LnCl_3$), murexid ($CuCl_2$), Patton and Reeder's reagent ($CaCl_2$), and Eriochrome Black T ($MgCl_2$, $MnCl_2$) as indicators. The concentration of the H_4DO3A−SA (prepared as described in ref 11) and H_3DO3A (Fluka) was determined by pH-potentiometric titration in the presence and absence of a large (40-fold) excess of $CaCl_2$. The pH-potentiometric titrations were made with standardized 0.2 M KOH.

Equilibrium Measurements. The stability and protonation constants of Mg^{2+}, Ca^{2+}, Mn^{2+}, Zn^{2+}, and Cu^{2+} complexes formed with DO3A−SA and DO3A ligands were determined by pH-potentiometric titration. The metal-to-ligand concentration ratio was 1:1 (the concentration of the ligand was generally 0.002 M). The protonation constants of the Ln(DO3A−SA) complexes were determined by pH potentiometry with the titrations of the preprepared Ln(HDO3A−SA) complexes from pH = 4.0 to pH = 11 with 0.2 M KOH. The stability constants of the Ln(DO3A−SA) and Ln(DO3A) complexes were determined by the "out-of-cell" technique because of the slow formation reactions. The pH range where the complexation equilibria existed and the time needed to reach the equilibria were determined by spectrophotometry for the formation of Ce(DO3A−SA). Eight Ln^{3+}-DO3A−SA and Ln^{3+}-DO3A samples were prepared, which had pH values in the range of 2.5−4.0 at equilibrium ($[Ln^{3+}] = [L] = 0.002$ M). The samples were kept at 25 °C for 6 weeks to reach equilibrium. For the calculations of the stability constants of the Ln(DO3A−SA) and Ln(DO3A) complexes, besides the protonation constants of ligands, the stability constants of the triprotonated *Ln(H_3DO3A−SA) and diprotonated *Ln(H_2DO3A) out-of-cage complexes (considered as intermediates in kinetics, see below) were also used as fixed values, which were calculated from the pH-potentiometric titration curves of

 dx.doi.org/10.1021/ic4025958 | *Inorg. Chem.* 2014, 53, 2858−2872

the Ln^{3+}-DO3A−SA and Ln^{3+}-DO3A systems obtained in the pH range of 1.7−4.0.

For the pH measurements and titrations, a Metrohm 785 DMP Titrino titration workstation and a Metrohm-6.0233.100 combined electrode were used. Equilibrium measurements were carried out at a constant ionic strength (0.1 M KCl) in 6 mL samples at 25 °C. The solutions were stirred, and N_2 was bubbled through them. The titrations were made in the pH range of 1.7−11.7. KH-phthalate (pH = 4.005) and borax (pH = 9.177) buffers were used to calibrate the pH meter. For the calculation of $[H^+]$ from the measured pH values, the method proposed by Irving et al. was used.[20] A 0.01 M HCl solution was titrated with the standardized KOH solution at 0.1 M KCl ionic strength. The differences between the measured (pH_{read}) and calculated pH ($-\log[H^+]$) values were used to obtain the equilibrium H^+ concentration from the pH values measured in the titration experiments.

The stability constants of the $Cu(DO3A-SA)^{2-}$ and $Cu(DO3A)^-$ complexes were determined by spectrophotometry studying the Cu^{2+}−DO3A−SA and Cu^{2+}−DO3A systems at $[H^+]$ = 0.03−1.0 M in the wavelength range of 400−800 nm. The concentrations of Cu^{2+}, DO3A−SA, and DO3A were 0.0015 M. The H^+ concentration in the samples was adjusted with the addition of calculated amounts of 3 M HNO_3. (The ionic strength was not constant in these samples.) The samples were kept at 25 °C for a week. The absorbance values of the samples were determined at 11 wavelengths. For the calculations of the stability and protonation constants, the molar absorptivities of $Cu(NO_3)_2$, Cu(DO3A−SA), Cu(HDO3A−SA), $Cu(H_2DO3A-SA)$, $Cu(H_3DO3A-SA)$, Cu(DO3A), Cu(HDO3A), and $Cu(H_2DO3A)$ were determined by recording the spectra of 1.0×10^{-3}, 1.5×10^{-3}, 2.0×10^{-3}, and 2.5×10^{-3} M solutions of $Cu(NO_3)$, Cu(DO3A−SA), and Cu(DO3A) in the pH range of 1.7−11.7. The protonation constants of Cu(DO3A−SA) and Cu(DO3A) complexes were also determined by pH-potentiometric titrations at a 1:1 metal-to-ligand molar ratio.

The protonation constants of the sulphonamide nitrogen of the DO3A−SA ligand and Ln(DO3A−SA) complexes were also determined by spectrophotometry at the absorption band of the aromatic group. The absorption spectra of the 0.1 mM solution of DO3A−SA ligand and Ln(DO3A−SA) complexes were recorded at pH = 4−12 in the wavelength range of 220−345 nm. The pH was adjusted by concentrated KOH or HCl. The spectrophotometric experiments were performed with a Cary 1E spectrophotometer in a 1 cm quartz cuvette at 25 °C. The protonation and stability constants were calculated with the PSEQUAD program.[21]

^{1}H NMR Relaxometry. The relaxivity values were calculated from the longitudinal relaxation time of H_2O protons (T_1) measured with a Bruker MQ20 minispec spectrometer at 20 MHz. The temperature of the sample holder was controlled with a thermostatted air stream. The longitudinal relaxation time was measured with the "inversion recovery" method (180° − τ − 90°) by using eight different τ values. The measurements were performed with a 1 mM solution of the Gd(DO3A−SA) complex, so the relaxivity values were given as $r_1 = 1/T_{1p} + 1/T_{1w}$ where T_{1p} and T_{1w} were the relaxation times of water protons in the presence and absence of the Gd(DO3A−SA) complex. For determining the stability constant of the Gd(DO3A−SA) complex, we measured the proton relaxation rates of "out-of-cell" samples prepared in the pH range of 2.5−4.0 ($[Gd^{3+}]$ = [L] = 0.002 M). In the equilibrium systems besides the free Gd^{3+} ions and GdL complexes, *$Gd(H_3L)$ out-of-cage complex (intermediate) was also present. Although its concentration was low (<15%), the contribution to the relaxivity was substantial, because in the intermediate, 4 or 5 water molecules are coordinated in the inner-sphere of Gd^{3+}. The relaxivity of the triprotonated *$Gd(H_3L)$ intermediate complex was calculated from the relaxivity versus time curve, obtained for the reaction of 1 mM Gd^{3+} with 10 mM of DO3A−SA at pH = 4.0 (20 MHz and 25 °C). The variable pH-relaxivity measurements of the Gd(DO3A−SA) complex were carried out by direct titration of the samples at higher pH values (4.5 < pH < 9.2; [Gd(DO3A−SA)] = 1.0 mM, 20 MHz, and 25 °C).

Kinetic Studies. Formation rates of Ce(DO3A−SA) and Eu(DO3A−SA) were studied by spectrophotometry at 290 and 255 nm, respectively. The formation of Yb(DO3A−SA) was monitored via the slow release of H^+ from the ligand by spectrophotometry at 616 nm in weakly buffered solutions with bromocresolgreen indicator (pK_a = 4.67 ± 0.02).[22] The formation rates were studied in the pH range of about 3.7−6.0. In the presence of 0.01 M buffer, the decrease of pH was approximately 0.07−0.1 pH unit. The concentration of DO3A−SA was 2×10^{-4} M. The formation of Ln^{3+} complexes have been studied in the presence of 5- to 50-fold Ln^{3+} excess in order to keep pseudo-first-order conditions. The pseudo-first-order rate constants ($k_{obs} = k$) were calculated by fitting the absorbance values to the eq 1:

$$A_t = (A_0 - A_e)e^{(-kt)} + A_e \quad (1)$$

where A_0, A_e and A_t are the absorbance values at the start, at equilibrium, and at a time t of the reaction, respectively.

The kinetic inertness of Gd(DO3A−SA) and Gd(DO3A) was characterized by the rates of the exchange reactions taking place between the complexes and Cu^{2+}. The transmetalation reactions were followed by spectrophotometry at the absorption band of the Cu(DO3A−SA) and Cu(DO3A) complexes at 300 nm in the pH range of 3.1−5.2. The concentration of Gd^{3+} complexes was 1×10^{-3} M, whereas the concentration of Cu^{2+} was 10 to 40 times higher. The pseudo-first-order rate constants ($k_d = k$) were calculated by fitting the absorbance data to eq 1.

The temperature was maintained at 25 °C, and the ionic strength of solutions was kept constant with 0.1 M KCl. In order to keep the pH values constant, 1,4-dimethylpiperazine (pH = 3.1−4.1), *N*-methylpiperazine (pH = 4.1−5.2), and piperazine (pH = 4.7−6.6) buffers (0.01 M) were used.

NMR Measurements. One-dimensional (1D) and two-dimensional (2D) NMR measurements were performed by a Bruker DRX 400 spectrometer (9.4 T) equipped with a Bruker VT-1000 thermocontroller using a 5 mm broad-band probe. The protonation of the DO3A−SA ligand was followed by ^{1}H NMR spectroscopy. A 0.01 M solution of the ligand in H_2O with 5% D_2O was prepared for these experiments. The pH was adjusted by stepwise addition of KOH and/or HCl (both prepared in H_2O). Calculation of the protonation constants was performed by the fitting of the chemical shift−pH data pairs with the computer program Micromath Scientist, version 2.0 (Salt Lake City, UT).

The structural behavior and the dynamic processes of the Ln(DO3A−SA) complexes were followed by 1D (^{1}H and ^{13}C) and 2D (COSY, NOESY and HSQC) NMR spectroscopy. In ^{13}C NMR spectroscopy, proton decoupling was used with an inverse-gated decoupling pulse program. The Ln(DO3A−SA) complexes were prepared in D_2O ([LnL] = 0.2 M). The chemical shifts are reported in ppm, with respect to TMS for ^1H and ^{13}C as an external standard (0 ppm for both cases). The COSY, NOESY, and HSQC spectra were collected by using gradient pulses in the z direction with the standard Bruker pulse programs. For NOESY spectra, the mixing time (D8) was 300 ms.

Computational Methods. All calculations were performed by employing hybrid DFT with the B3LYP exchange correlation functional[23,24] and the Gaussian 09 package.[25] Full geometry optimizations of the Ln(DO3A−SA) complexes were performed in vacuo and also in PCM[26,27] by using the 6-31G(d) basis set for carbon, hydrogen and 6-31+G(d) for nitrogen, oxygen, and sulfur atoms. Different computational studies on lanthanide(III) complexes indicated that the 4f orbitals did not participate in bonding.[28−30] Therefore, in the case of lanthanides, the quasi-relativistic effective core potential (ECP) of Dolg et al. and the related [5s4p3d]-GTO valence basis sets were applied.[31] This ECP treated $[Kr]4d^{10}4f^n$ as fixed cores, although only the $5s^25p^66s^25d^16p^0$ shell was taken into account explicitly.

The nature of the stationary points (intermediates and transition states) was characterized by frequency analysis. The relative energy barriers calculated in vacuo and PCM include zero-point energies obtained by frequency analysis.

X-ray Diffraction Experiments. Single-crystal X-ray diffraction data were collected at 293 (1) K with an Enraf Nonius MACH3 diffractometer, Mo Kα radiation λ = 0.71073 Å, ω motion. Raw data were evaluated using the XCAD4 software,[32] and the structure was solved using direct methods[33] and refined on F^2 using the SHELX-97 program.[34] The Platon package[35] was used for crystallographic calculations, and publication material was prepared with the WINGX-97 suite.[36] Blue-colored prism (0.35x 0.25 × 0.12 mm) crystals of $C_{23}H_{35}CuN_5O_9S$, M_w = 621.16, monoclinic, a = 21.913(4) Å, b = 9.224(2) Å, c = 12.878(2) Å, β = 99.17(5), V = 2570(8) Å^3, Z = 4; space group: $P21/c$ (no. 14), ρ_{calc} = 1.606 g cm^{-3}; θ_{max} = 25.3°, 5115 measured reflections, of which 4664 were independent and 3156 were unique with $I > 2\sigma(I)$, decay: 5%, $R(F)$ = 0.063 and w$R(F^2)$ = 0.167 for 4664 reflections, 359 parameters, 2 restraints. Residual electron density = 1.17/−0.63 e/Å^3, close to the copper atom. Heavy atoms were refined anisotropically. Hydrogen atoms were treated with a mixture of independent and constrained refinement. The difference electron density map clearly shows the position of the carboxylate proton. Hydrogen atoms of the methyl group were refined using a riding model.

■ RESULTS AND DISCUSSION

A great number of macrocyclic ligands and Gd^{3+} complexes have been synthesized during the last two decades in order to develop new responsive contrast agents. Thermodynamic stability, kinetics, relaxation properties, solution structures, and dynamics of their Gd^{3+} complexes were studied to evaluate the suitability of the ligands and usually compared with those of Gd(DOTA) or Gd(DO3A). The trend of the stability constants of the DOTA derivative complexes in the lanthanide series is generally similar. The logK_{LnL} values increase from La^{3+} to the middle of the series, and the stability constants of the heavier lanthanides are nearly identical.[37] The stability constants (logK_{LnL}) of the octadentate DOTA complexes are generally 3−4 orders of magnitude higher than those of the complexes of the heptadentate ligands, like DO3A.[5,14,38,39] The behavior of the DO3A−SA in this respect seems to be peculiar, because at lower pH (pH < 5), it is a heptadentate ligand, whereas at higher pH (pH > 9) it proved to be octadentate in the complexes of lanthanides. The characterization of the equilibrium properties of DO3A−SA has been started by determining the protonation constants.

Protonation Equilibria of H_4DO3A−SA and H_3DO3A Ligands. The complexation properties and protonation equilibria of the H_4DO3A−SA have not been studied previously. The definitions and equations used for the evaluation of the equilibrium data are summarized in the Supporting Information. The logK_i^H values obtained by pH-potentiometry, ^1H NMR spectroscopy, and UV-spectrophotometry are listed and compared with those of H_3DO3A and H_4DOTA in Table 1. Standard deviations (3σ) are shown in parentheses.

Table 1. Protonation Constants of DO3A−SA, DO3A, and DOTA at 25°C

	DO3A−SA[a]		DO3A	DOTA[b]
I	0.1 M KCl		0.1 M KCl	0.1 M KCl
method	pH-pot.	^{1}H NMR	pH-pot.	pH-pot.
logK_1^H	12.34 (2)	12.56 (3)	11.99 (2)	11.41
logK_2^H	11.02 (2)	11.13 (4)	9.51 (2)	9.83
logK_3^H	9.22 (2)	9.26 (3)	4.30 (2)	4.38
logK_4^H	4.43 (2)	4.38 (9)	3.63 (2)	4.63
logK_5^H	2.60 (2)	2.52 (3)	1.84 (2)	1.92
logK_6^H	1.52 (3)			1.58
Σ logK_i^H	41.13	39.85	31.26	33.75

[a]Protonation constant of sulphonamide nitrogen of DO3A−SA determined by UV-spectrophotometry is logK_{NH} = 11.15 (5), 0.1 M KCl, 25 °C. [b]ref 40.

Comparison of the protonation constants of DO3A−SA with those of DOTA and DO3A obtained in 0.1 M KCl indicates that the logK_1^H value of DO3A−SA is somewhat higher, whereas its logK_3^H, logK_4^H, and logK_5^H values are comparable with those of logK_2^H, logK_3^H, and logK_4^H values of the DOTA and DO3A. The higher first protonation constant of DO3A−SA might be explained by the H-bond formation between the protonated ring nitrogen and the deprotonated sulphonamide N^- atom. The protonation constant of the sulphonamide N^- atom logK_2^H = 11.02 (2) is similar to that of a DOTA derivative ligand containing a dansyl group (logK_{NH} = 10.8).[41] The ΣlogK_i^H value of DO3A−SA ligand is higher than that of the DOTA and DO3A, which is related to the basic N^- atom of the sulphonamide pendant arm. On the basis of this finding, one can expect higher stability for the DO3A−SA complexes compared to those of DOTA or DO3A if the sulphonamide group is involved in the metal−ligand interaction (i.e., when the deprotonated N^- donor atom is coordinated).

Complexation Equilibria of DO3A−SA and DO3A. The stability and protonation constants of the complexes of DO3A−SA and DO3A formed with several metal ions are presented in Table 2. The stability constants of the protonated *Ln(H_iL) out-of-cage (intermediate) complexes (log*$K_{Ln(HiL)}$ values) are also presented in Table 2 in the columns MH_3L for DO3A−SA and MH_2L for the DO3A, respectively. The stability constants obtained for the DO3A−SA and DO3A

Table 2. Stability ($\log K_{ML}$) and Protonation ($\log K_{MH_iL}$) Constants of Metal Complexes Formed with DO3A–SA, DO3A, and DOTA Ligands (25°C)

I	DO3A–SA				DO3A			DOTA
	0.1 M KCl				0.1 M KCl			0.1 M KCl
	ML	MHL	MH_2L	MH_3L	ML	MHL	MH_2L	ML
Mg^{2+}	11.87 (4)	10.93 (3)			11.64 (3)			11.49 (3)
Ca^{2+}	13.68 (3)	10.64 (2)	5.20 (3)		12.57 (1)	4.60 (9)		16.11 (1)
Zn^{2+}	21.79 (2)	10.29 (2)	3.74 (2)	2.99 (1)	21.57 (1)	3.47 (1)	2.07 (1)	20.21 (1)
Cu^{2+}	26.27 (6)	10.14 (1)	3.97 (2)	2.00 (2)	25.75 (7)	3.65 (2)	1.69 (6)	24.83[b]
Mn^{2+}	20.10 (5)	10.30 (1)	3.56 (1)	2.93 (1)	19.43 (1)	3.37 (3)		19.44 (3)
La^{3+}	21.58 (7)	7.23 (5)		4.42 (2)[a]	18.63 (8)		6.27 (2)[a]	21.7[c]
Ce^{3+}	22.00 (3)	6.93 (3)		4.45 (1)[a]				23.4[c]
Nd^{3+}	22.56 (9)	6.65 (5)		4.47 (1)[a]				23.0[c]
Gd^{3+}	23.45 (9)	6.16 (2)		4.43 (1)[a]	21.56 (8)		5.93 (2)[a]	24.7[c]
Dy^{3+}	23.55 (9)	6.02 (5)		4.50 (2)[a]				24.8[c]
Er^{3+}	23.58 (9)	6.23 (5)		4.59 (2)[a]				24.5 (Tm^{3+})[c]
Lu^{3+}	23.65 (7)	6.97 (2)		4.64 (1)[a]	21.44 (8)		5.69 (3)[a]	25.4[c]

[a]Stability constants of the protonated *$Ln(H_iL)$ out-of-cage complex (intermediate) *$K_{Ln(HiL)} = [Ln(HiL)]/[Ln^{3+}][H_iL]$, where $i = 3$ for DO3A–SA and $i = 2$ for DO3A. [b]Ref 40. [c]Ref 42 (0.1 M NaCl, 25 °C); Cu(DO3A–SA): $\log K_{CuL} = 26.35$ (2), $\log K_{CuHL} = 10.30$ (3), Y(DO3A–SA): $\log K_{LnHL} = 6.58$ (4), Cu(DO3A): $\log K_{CuL} = 25.98$ (3), $\log K_{CuH2L} = 1.81$(2) by spectrophotometry; Gd(DO3A–SA): $\log K_{GdL} = 23.36$ (8); $\log K_{GdHL} = 6.21$ (2) by relaxometry (0.1 M KCl, 25 °C).

complexes are compared with those of the DOTA complexes in Table 2.

The stability constant $\log K_{CuL} = 25.75$ (7) obtained for the $Cu(DO3A)^-$ is significantly higher than the similar data ($\log K_{CuL} = 22.87$) published earlier in literature.[43] The probable reason of this large difference is that the authors did not consider the formation of the protonated $Cu(H_2L)$ species. Kaden et al. also determined the stability constant of Cu(DO3A) complex and they obtained the value $\log K_{CuL} = 26.49$,[39] which is close to our $\log K_{CuL} = 25.75$ value. The stability and protonation constant of the Cu(DO3A–SA) and Cu(DO3A) determined by pH-potentiometry (Table 2) agree well with those obtained by spectrophotometry (presented under the Table 2).

The stability constants of the Ca^{2+} and Ln^{3+} complexes formed with DO3A–SA and DO3A (Table 2) are generally about 1–2 orders of magnitude lower than those of the corresponding DOTA complexes. The $\log K_{ML}$ values determined for the Mg^{2+}, Zn^{2+}, Cu^{2+}, and Mn^{2+} DO3A–SA complexes are similar to those of DO3A and even higher than the stability constants of the corresponding DOTA complexes. This is surprising, because the total basicity of the DO3A is lower and it has one donor atom less than DOTA. The stability constants of the Cu^{2+} and Zn^{2+} complexes of DO3A–SA and DO3A are about 1.5 orders of magnitude higher than those of Cu(DOTA) and Zn(DOTA). The higher stability may be explained in terms of the optimal wrapping of the ligand around the Cu^{2+} and Zn^{2+} ion in DO3A–SA and DO3A complexes. However, the similar stability of DO3A–SA and DO3A complexes of Zn^{2+} and Cu^{2+} indicates that the sulphonamide pendant arm does not participate in the coordination, because the coordination number of metal ions is lower than the number of donor atoms in the ligands.

The stability constants of the Ln(DO3A–SA) complexes increase from La^{3+} to Gd^{3+} and then remain practically constant for the heavier lanthanides (Table 2). Similar trends were found for the Ln(DO3A) and Ln(DOTA) complexes, too. This result clearly indicates that the size match between the Ln^{3+} ions and the coordination cage determined by the ring nitrogens and the carboxylate oxygens of the ligand is optimal at the middle of the Ln^{3+} series.

The protonation constants of the sulphonamide nitrogen of the free ligand ($\log K_2^H$, Table 1) and the complexes of Mg^{2+}, Ca^{2+}, Mn^{2+}, Zn^{2+}, and Cu^{2+} ($\log K_{MHL}$, Table 2) are similar, which indicates that the deprotonated sulphonamide N^- atom is not or very weekly coordinated to the M^{2+} divalent metal ions. However, the protonation constants ($\log K_{LnHL}$) of the sulphonamide nitrogen of the Ln(DO3A–SA) complexes were found to be in the range of 6.0–7.3, which is 4–5 orders of magnitude lower than the protonation constant of the free DO3A–SA. It means that the interaction between the Ln^{3+} ions and the sulphonamide N^- is strong, and this binding is responsible for the higher $\log K_{LnL}$ values of the Ln(DO3A–SA) complexes compared to those of the Ln(DO3A) complexes. The protonation constants ($\log K_{LnHL}$) of the sulphonamide nitrogen of the Ln(DO3A–SA) complexes show a minimum curve in the lanthanide series (Table 2). In the first half of lanthanide series, the decrease of the $\log K_{LnHL}$ values can be explained by an increasing interaction between the sulphonamide group and the Ln^{3+} ions due to its increased charge density. For the second half of the series, some steric hindrance between the coordinated carboxylate and the bulky sulphonamide group is probably balancing and even canceling the previous effect.

The Ca^{2+}, Zn^{2+}, Cu^{2+}, and Mn^{2+} complexes of DO3A–SA and DO3A, similarly to those of DOTA, form di- and triprotonated species at lower pH values (Table 2). In these complexes, one carboxylate group is free, and it is protonated at pH around 3–5. At lower pH values, another carboxylate group can be protonated, forming triprotonated complexes.

Solid State Structure of the $Cu(H_2DO3A–SA)$ Complex. The X-ray structure of $Cu(H_2DO3A–SA)$ is shown in Figure 1 with the selected bond length data. The coordination around Cu^{2+} is distorted octahedral attributed to the Jahn–Teller effect. The coordination sites of Cu^{2+} are occupied by two of the ring N-atoms (N4, N10) and two carboxylate O-atoms (O10, O31) in a square planar fashion in equatorial position. The other two N-atoms (N1, N7) of the ring in axial position complete the coordination sphere. The solid state

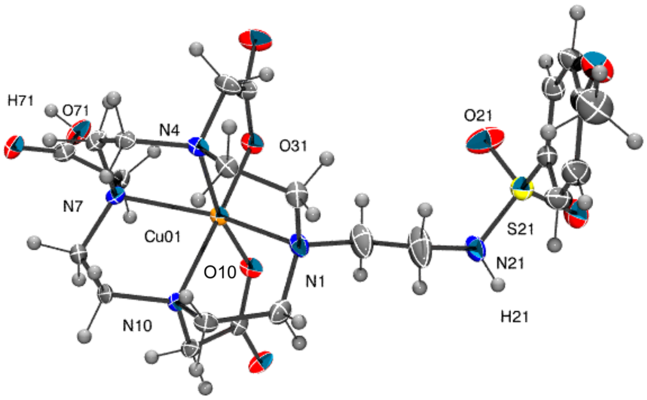

Figure 1. ORTEP view of Cu(H_2DO3A−SA) complex at 50% probability level with numbering scheme. Selected bond length (Å) data: Cu01−N1 2.294 (6); Cu01−N4 2.085 (5); Cu01−N7 2.306 (6); Cu01−N10 2.090 (5); Cu01−O10 1.942 (4); Cu01−O31 1.950 (4).

structure also indicates that the carboxylate O atom (O71) and the sulphonamide nitrogen are protonated and noncoordinated. The distance of the Cu^{2+} ion from the N4−N10−O10−O31 and N1−O31−N7−N10 least-squares plane is 0.019 and −0.122 Å, respectively, with an angle of 88.8°, whereas the N1−Cu01−N7 angle is 152.6(2)°. Other details regarding the structure of Cu(H_2DO3A−SA) are summarized in the Supporting Information. The solid-state structure of the Cu(H_2DO3A−SA) is very similar to that of the analogues Cu(H_2DOTA) complex (two opposite carboxylate oxygen atoms are protonated), the coordination of Cu^{2+} is completed by two carboxylate oxygen and the two ring nitrogen atoms in the equatorial plane and by two ring nitrogen atoms in the axial positions.[44] In the equatorial plane, the Cu−N and Cu−O distances are 2.107 and 1.966 Å, whereas the Cu−N distances are 2.319 Å in axial positions.[44]

Formation Kinetics of Ln(DO3A−SA) Complexes. The complex formation reactions between the DO3A−SA ligand and Ln^{3+} ions are slow at pH around 4−6. Because the formation reactions of the Ln^{3+} complexes with open-chain ligands are generally fast, the slow formation of Ln(DO3A−SA) complexes can be attributed to the macrocyclic ligand similarly to that of the Ln(DOTA).[45−49]

The kinetic studies were performed in the pH range of 3.7−6.0, where mainly the Ln(HDO3A−SA) species formed (Table 2). The formation rate of the Ln(HDO3A−SA) complexes in the presence of Ln^{3+} excess can be expressed by eq 2

$$\frac{d[\mathrm{LnHL}]_t}{dt} = k_{obs}[L]_t \qquad (2)$$

where k_{obs} is a pseudo-first order rate constant, $[L]_t$ is the total concentration of the H_xDO3A−SA ligand and $[\mathrm{LnHL}]_t$ is the total concentration of complexes containing the species LnL at any time. The k_{obs} values obtained for the formation reactions of the Ce^{3+}−, Eu^{3+}−, and Yb^{3+}−DO3A−SA complexes are shown in Figure S9. The saturation curves indicate the fast formation of a reaction intermediate which slowly rearranges to the product, Ln(HDO3A−SA), like in the formation reactions of the Ln(DOTA) complexes.[45,49,50] In the intermediate, presumably only three acetate groups are coordinated to the Ln^{3+} ion outside of the coordination cage of the ligand, which is protonated at two diagonal ring nitrogen and the sulphonamide nitrogen atoms. The rate-controlling step is the loss of the last proton from the ring nitrogens.[45,50] Considering the saturation curves, the dependence of the k_{obs} values on the Ln^{3+} concentration can be expressed by eq 3.

$$k_{obs} = \frac{k_f{}^*K^c_{\mathrm{Ln(H_3L)}}[\mathrm{Ln}^{3+}]}{1 + {}^*K^c_{\mathrm{Ln(H_3L)}}[\mathrm{Ln}^{3+}]} \qquad (3)$$

where k_f is the rate constant for the formation of the product by the deprotonation and rearrangement of the intermediate. ${}^*K^c_{\mathrm{Ln(H_3L)}}$ is the equilibrium constant, characterizing the formation of the intermediate.[51] By fitting the k_{obs} data to eq 3, the k_f and ${}^*K^c_{\mathrm{Ln(H_3L)}}$ values have been calculated. The conditional stability constants of the *Ce(H_3L), *Eu(H_3L), and Yb(H_3L) intermediates ($\log{}^*K^c_{\mathrm{Ln(H3L)}}$) calculated from the kinetic data are 3.24 ± 0.02, 3.15 ± 0.02, and 3.21 ± 0.01, respectively. These values are comparable with the equilibrium constant of the diprotonated *Gd(H_2DO3A) intermediate (3.48)[52] and somewhat lower than those reported for the *Ln(H_2DOTA) intermediates (Ce^{3+}: 4.4; Eu^{3+}: 4.3; Yb^{3+}: 4.2),[45] which indicates that the structure and the number of the acetate arms coordinating to the Ln^{3+} ion in *Ln(H_3DO3A−SA) are similar to those of the *Ln(H_2DO3A) intermediates. The obtained k_f rate data are directly proportional to the OH^- concentration (Figure 2), which can be expressed by eq 4

$$k_f = k_{OH}[\mathrm{OH}^-] \qquad (4)$$

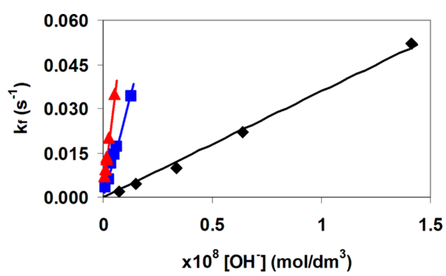

Figure 2. Rate constants (k_f) of the formation reactions of Ln(HDO3A−SA) complexes as a function of $[\mathrm{OH}^-]$ for Ce^{3+} (black diamond), Eu^{3+} (blue squares), and Yb^{3+} (red triangle) (0.1 M KCl, 25 °C).

Similar rate expressions were obtained for the formation reactions of the DOTA and DOTA derivative complexes of lanthanides.[46,49,50,52,53] The calculated k_{OH} rate constants are presented in Table 3, where some data known for the other DOTA derivative complexes are also shown. The comparison of the k_{OH} values shows that the presence of the sulphonamide group has no role in the formation reactions of the Ln(HDO3A−SA) complexes.

Dissociation Kinetics of the Gd(DO3A−SA) and Gd(DO3A). The lanthanide complexes used in medical diagnosis and therapy must have high kinetic inertness, because the products of dissociation, the free Ln^{3+} ion, and the ligands are toxic.[2] The dissociation of the Ln^{3+} complexes formed with DOTA and DOTA derivative ligands is very slow and occurs via a proton-assisted pathway, and the endogenous metal ions like Zn^{2+} and Cu^{2+} have no effect on the dissociation rates.[45,54,55] In this work, the metal exchange reactions of Gd(DO3A−SA) and Gd(DO3A) complexes with Cu^{2+} have been investigated at high Cu^{2+} concentrations (10−40-fold excess) in order to guarantee pseudo-first-order conditions. The metal exchange reaction of Gd(DO3A−SA) and Gd(DO3A) with Cu^{2+} (eq 5) has been followed by spectrophotometry on

Table 3. Rate Constants, k_{OH} (M^{-1} s^{-1}), for the Deprotonation and Rearrangement of *Ce(H_3DO3A−SA), *Eu(H_3DO3A−SA), and *Yb(H_3DO3A−SA) Intermediates to the Final Ln(HDO3A−SA) Complexes (0.1 M KCl, 25°C) Together with Literature Data for Comparison

	Ce^{3+}	Eu^{3+}	Yb^{3+}
DO3A−SA	$(3.6 \pm 0.1) \times 10^6$	$(2.7 \pm 0.1) \times 10^7$	$(6.2 \pm 0.2) \times 10^7$
DOTA[a]	3.5×10^6	1.1×10^7	4.1×10^7
DO3A−Butrol[b]	2.1×10^6	4.8×10^6	1.6×10^7
DO3A[c]		2.1×10^7 (Gd^{3+})	
DO2A[b]	2.8×10^5		2.5×10^5

[a]Ref 45, [b]Ref 53, [c]Ref 52.

Table 4. Rate Constants and Half-Lives ($t_{1/2} = \ln2/k_d$) Characterizing the Dissociation Reactions of Gd(HDO3A−SA), Gd(DO3A), and Gd(DOTA) Calculated from the Transmetallation Reactions with Cu^{2+} (25°C)

	Gd(HDO3A−SA)	Gd(DO3A)		Gd(DOTA)[b]
I	0.1 M KCl	0.1 M KCl	1.0 M KCl[a]	0.15 M NaCl
k_0 (s^{-1})	$(-6 \pm 20) \times 10^{-10}$	$(-2 \pm 20) \times 10^{-9}$		6.7×10^{-11}
k_1 (M^{-1} s^{-1})	0.86 ± 0.01	$(2.3 \pm 0.1) \times 10^{-2}$	2.5×10^{-2}	1.8×10^{-6}
k_d (s^{-1}) at pH = 7.4	3.4×10^{-8}	9.2×10^{-10}	1.0×10^{-9}	7.3×10^{-14}
[c]$t_{1/2}$ (h) at pH = 7.4	5.6×10^3	2.1×10^5	1.9×10^5	2.7×10^9

[a]Ref 56, [b]Ref 54, [c]$t_{1/2} = \ln2/k_d$.

the absorption band of the Cu(DO3A−SA) and Cu(DO3A) at 320 nm in the pH range of 3.2−5.2.

$$GdH_iL + Cu^{2+} \rightleftharpoons CuL + Gd^{3+} + iH^+ \quad (5)$$

where i = 1 and 0 for the Gd(DO3A−SA) and Gd(DO3A), respectively. The rates of the exchange reactions can be expressed by eq 6

$$-\frac{d[GdL]_t}{dt} = k_d[GdL]_t \quad (6)$$

where k_d and $[GdL]_t$ are a pseudo-first-order rate constant and the total concentration of the GdL complexes. Some typical absorption spectra of the Gd(HDO3A−SA)−Cu^{2+} and Gd(DO3A)−Cu^{2+} reacting systems are shown in Figures S10 and S11. The k_d values obtained are directly proportional to the H^+ concentration and independent of the Cu^{2+} concentration, as shown Figure S13. These findings show that the exchange reactions (5) occur through the proton-assisted dissociation of complexes, followed by the fast reaction of the free ligands with Cu^{2+}. This reaction pathway is characterized by the rate constant k_1. It can be assumed that the dissociation may occur as a spontaneous reaction, characterized by the rate constant k_0. Considering both possible reaction pathways, the k_d values in eq 6 can be expressed by eq 7

$$k_d = k_0 + k_1[H^+] \quad (7)$$

On the basis of the k_d values presented in Figure S12, the k_0 and k_1 values for the reactions of Gd(HDO3A−SA) and Gd(DO3A) have been calculated and presented in Table 4. For comparison, the k_0 and k_1 values known for the reactions of other DOTA derivative complexes are also shown.

As shown in Table 4, the k_0 rate constants are very small, and the errors obtained by the calculations are very large, which indicate that the spontaneous dissociation of the Gd(HDO3A−SA) and Gd(DO3A) complex does not contribute to the transmetalation reactions. The rate data presented in Table 4 also show that the k_1 value of Gd(HDO3A−SA) is much higher than that of Gd(DO3A) or Gd(DOTA). The kinetic behavior of Gd(HDO3A−SA) and Gd(DO3A) is expected to be similar to that of Ln(DOTA) complexes, so the interpretation of kinetic data (Table 4) can also be similar.[45,54,55] The protonation of the Ln(DOTA) and Ln(DO3A) complexes probably occurs at the carboxylate group.[45,56] The protonation of Gd(HDO3A−SA) presumably starts also on a carboxylate with the temporary formation of a free −COOH group. For the dissociation of complexes, the proton must be transferred to the ring nitrogen, forcing the Gd^{3+} ion to leave the coordination cavity. The proton transfer is more likely if the complex is less rigid (e.g., Ln(DO3A) complexes which can dissociate much faster than the Ln(DOTA) complexes).[45,54,56] Besides, the rate data we obtained here characterize the inertness of the Gd(HDO3A−SA) complex containing protonated and noncoordinated sulphonamide group. Because the protonation constant of the sulphonamide group of the deprotonated Gd(DO3A−SA) is $\log K_{GdHL}$ = 6.16, at physiological pH, the ligand is essentially coordinated as an octadentate ligand due to the coordination of the sulphonamide N^- atom and the kinetic inertness of the Gd(DO3A−SA)$^-$ complex being expectedly much higher than that of the Gd(HDO3A−SA). (At pH = 7.4, 94% of the complex is in deprotonated Gd(DO3A−SA) form and only 6% is protonated.) In Table 4, the half-lives of dissociation for the complexes are also presented. This $t_{1/2}$ value of Gd(HDO3A−SA) is higher than the half-lives of dissociation of the open-chain complexes, Gd(DTPA-BMA) or Gd(DTPA) ($t_{1/2}$ = 50 h and $t_{1/2}$ = 305 h, respectively),[54] which means that the Gd^{3+} complexes formed with the arylsulphonamide group containing DOTA derivatives are promising for biological applications.

^{1}H and ^{13}C NMR Studies of the Ln(DO3A−SA) Complexes. Because the equilibrium, kinetic, and relaxation behaviors of Gd(DO3A−SA) complex are suitable for in vivo pH measurement, the structural properties have been thoroughly studied to obtain information about the relationship between the molecular parameters of the protonated Gd(HDO3A−SA) and deprotonated Gd(DO3A−SA) complexes and their ability to accelerate the longitudinal or transversal relaxation rate of water protons. The structural and dynamic properties of the deprotonated Ln(DO3A−SA) complexes have been investigated by multinuclear NMR spectroscopy.

dx.doi.org/10.1021/ic4025958 | Inorg. Chem. 2014, 53, 2858−2872

The solution structure of Ln(DO3A−SA) complexes is expected to be similar to that of the corresponding Ln(DOTA) complexes, which were studied in solid sate by the X-ray diffraction method and in solution by ^{1}H and ^{13}C NMR spectroscopy.[57−65] It is well-known that in Ln(DOTA) complexes the four ethylenediamine groups adopt identical helicities, which leads to two macrocyclic ring conformations: ($\delta\delta\delta\delta$) and ($\lambda\lambda\lambda\lambda$). The acetate groups are accommodated similarly (absolute configuration Δ or Λ), resulting in four possible steroisomers, existing as two enantiomeric pairs ($\Delta(\lambda\lambda\lambda\lambda)/\Lambda(\delta\delta\delta\delta)$ and $\Lambda(\lambda\lambda\lambda\lambda)/\Delta(\delta\delta\delta\delta)$). For the enantiomer pair $\Delta(\lambda\lambda\lambda\lambda)$ and $\Lambda(\delta\delta\delta\delta)$, the twist angle between the planes of four nitrogen and four oxygen is about 40°, corresponding to a square antiprismatic geometry (SAP), whereas the $\Lambda(\lambda\lambda\lambda\lambda)$ and $\Delta(\delta\delta\delta\delta)$ enantiomers have a twist angle of about −30°, which represents a twisted square antiprismatic geometry (TSAP). The SAP and TSAP isomers may interconvert in solution by either ring inversion ($\delta\delta\delta\delta \rightleftharpoons \lambda\lambda\lambda\lambda$) or arm rotation ($\Delta \rightleftharpoons \Lambda$) processes. Either process alone interconvert SAP and TSAP geometries, while a combination of the two processes exchanges enantiomeric pairs.[62−65] The molar fraction of the SAP and TSAP isomers is effected by the size of the Ln^{3+} ions. The amount of the SAP and TSAP isomers for Nd(DOTA) is equal, whereas for the lighter La^{3+}-, Ce^{3+}-, and Pr(DOTA), one isomer (likely the TSAP) is more abundant. For the heavier Ln^{3+} ions, the main species have a SAP structure.[62,65]

^{1}H NMR studies of the solution structure of Eu(DO3A−SA) published by Lowe et al. reveal that the resonances for the most-shifted ring axial protons at 37.5, 30.7, 27.9, and 18.9 ppm, correspond to the monocapped square-antiprismatic (SAP) coordination environment around the europium center.[11] The solid-state structure of the Y^{3+} complex formed with DOTAM−dansyl ligand is monocapped square-antiprismatic (SAP), and the Y^{3+} ion is nine-coordinated by four ring nitrogens, three amide oxygens, the sulphonamide N^{-}, and the oxygen donor atoms that is in a capping position (DOTAM = 1,4,7,10-tetraazacyclododecane-1,4,7,10 tetraacetamide).[66] By taking into account the similarity of the dansyl and arylsulphonamide groups, it can be assumed that the deprotonation and coordination of the sulphonamide N^{-} atom results in the coordination of the sulphonamide oxygen atom in Ln(DO3A−SA) complexes.

The solution structure of Ln(DO3A−SA) complexes is strongly related to the deprotonation and coordination of the sulphonamide NH group, which expectedly increases the rigidity of the Ln^{3+} complexes. It can be assumed that the solution structure of the protonated Ln(HDO3A−SA) looks highly like the corresponding Ln(DO3A) complexes. The deprotonation and coordination of the sulphonamide−NH−SO_2 group to the Ln^{3+} ion results in C_1 symmetry where 29 ^{1}H NMR resonances and 19 ^{13}C NMR resonances are expected. The ^{1}H NMR spectra of the deprotonated and protonated Eu(DO3A−SA), recorded at 270 K, are shown in Figure 3. It is seen that the ^{1}H NMR spectrum of the protonated Eu(HDO3A−SA) contains several broad signals, which indicates the fast fluctional motion of the Eu^{3+} complex even at low temperature. However, the ^{1}H NMR spectrum recorded at pH = 9.9 contains two sets of well-separated signals, indicating the presence of two isomers and the relatively rigid structure of the deprotonated Eu(DO3A−SA) complex (Figure 3). The variable temperature ^{1}H NMR spectra of the deprotonated Eu(DO3A−SA) are shown in Figure S13.

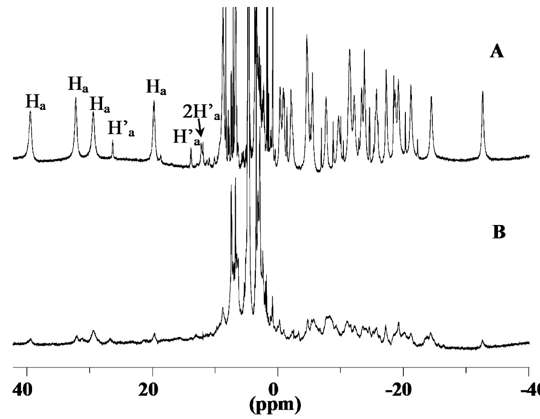

Figure 3. ^{1}H NMR spectra (500 MHz) of Eu(DO3A−SA) in D_2O at pD = 9.9 (A) and 5.1 (B), 270 K.

The chemical shifts of the axial ring protons of the major (H_a: 39.55, 32.31, 29.53, and 19.83 ppm) and minor (H'_a: 26.42, 13.96, 12.31, and 11.99 ppm) isomers of deprotonated Eu(DO3A−SA) are similar to those of the **M**ajor (SAP) and **m**inor (TSAP) isomers of Eu(DOTA), respectively. By comparison of the integrals for the two sets of axial ring protons, it is estimated that under these conditions, 86% of the Eu(DO3A−SA) exists as the SAP and 14% as TSAP isomer. This ratio is very close to the population ratio of the SAP and TSAP isomers of Eu(DOTA) obtained at 298 K.[62,65] At 273K, the ^{1}H NMR spectrum of the La(DO3A−SA) contains only one set of signals (Figure 4), which means the presence of one isomer. However, the ^{1}H NMR and EXSY spectra of Y(DO3A−SA) and Lu(DO3A−SA) recorded at 273 K (Figures S14−S17) reveal two sets of signals for the aromatic protons (Y(DO3A−SA): i' = 7.58 and 7.57 ppm; i = 7.47 and 7.45 ppm; j' = 6.92 and 6.90 ppm; j = 6,79 and 6.77 ppm; Lu(DO3A−SA): i' = 7.58 and 7.56 ppm; i = 7,46 and 7.44 ppm; j' = 6.91 and 6.90 ppm; j = 6,78 and 6.76 ppm) and the chemical exchange between the i and i' as well as j and j' protons, which can be interpreted by the formation and the exchange processes for both SAP and TSAP isomers. By taking into account the coordination of the sulphonamide O-atoms to the Ln^{3+} ions, two diastereomers of the SAP and TSAP isomers can be formed with the different orientation of the aromatic group. However, the ^{1}H NMR spectra of La(DO3A−SA), Y(DO3A−SA), and Lu(DO3A−SA) (Figures 4, S14 and S15) contain one set and two sets of signals, which indicates that the exchange between the coordinated and noncoordinated sulphonamide oxygen atoms is presumably fast on the actual NMR time scale. The negative charge of the deprotonated and the coordinated sulphonamide group might be delocalized between the sulphonamide group and the aromatic π electron system with the formation of mesomers. The chemical exchange between the mesomer structures explains the cross peak between i and j protons in the NOESY spectra (Figures S16 and S17). On the basis of the similarities of Ln(DOTA) and Ln(DO3A−SA) complexes, we assume that 100% of La(DO3A−SA) is present as TSAP, whereas about 93% of Y(DO3A−SA) and Lu(DO3A−SA) are present as SAP isomer (calculated from the integral values of the aromatic protons of the major and minor isomers). The La(DOTA) and Lu(DOTA) complexes form 100% TSAP and 82% SAP/18% TSAP isomers, respectively.[65] The relative distributions of the SAP and TSAP isomers of Ln(DO3A−SA) complexes indicate

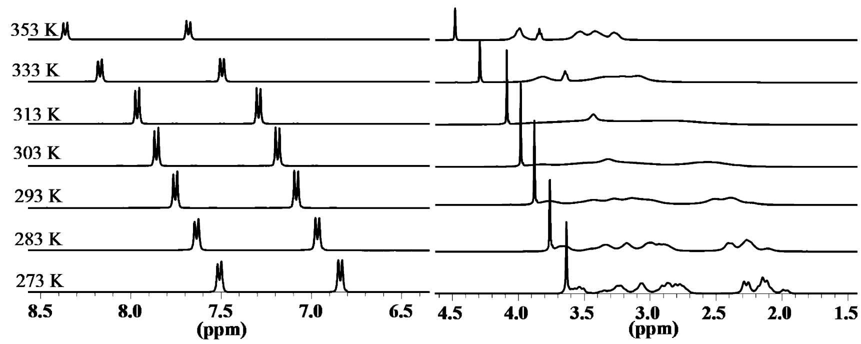

Figure 4. Variable temperature 400 MHz ^{1}H NMR spectra of La(DO3A−SA) at pDH = 10.3 in D_2O ([LaL] = 0.2 M).

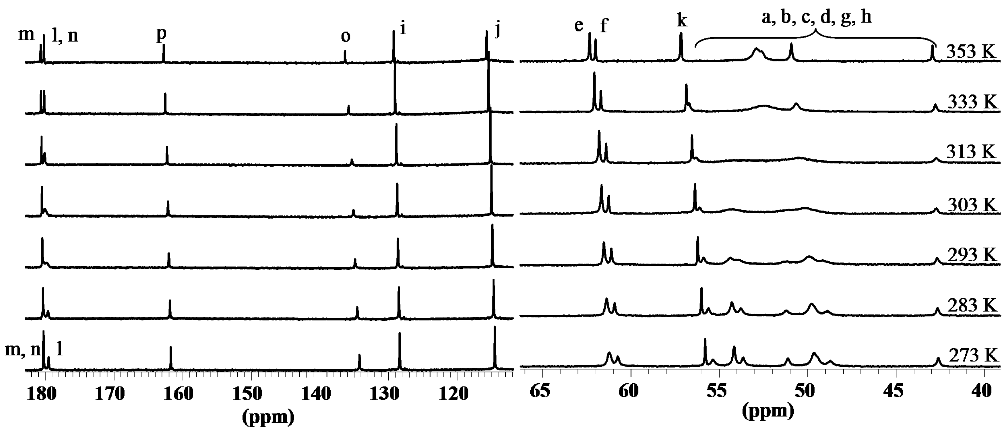

Figure 5. Variable temperature 100 MHz ^{13}C NMR spectra of La(DO3A−SA) at pH = 10.3 in D_2O ([LaL] = 0.2 M).

that the Ln(DO3A−SA) complexes of larger Ln^{3+} ions have the TSAP structure, whereas the SAP structure is preferred by Ln(DO3A−SA) complexes formed with the Ln^{3+} ions of smaller size. Indeed, the increasing population of the SAP isomer along the series is a general trend observed for the Ln(III) complexes of cyclen-based ligands due to an increased binding energy between donor atoms of the ligand and the Ln^{3+} ions of higher charge density in the SAP isomer against the TSAP one.[67] Moreover, the abundance of the SAP/TSAP isomer ratio of the Ln(DO3A−SA) complexes has been supported by the fact that the twist angle between the planes formed by the four ring nitrogens and three carboxylate oxygens and the relatively larger sulphonamide N^{-} group can provide the optimal size match with −30° for the larger Ln^{3+} ions and with 40° for the smaller Ln^{3+} ions.

The ^{1}H NMR spectra of Ln(DO3A−SA) complexes are very complicated due to C_1 symmetry, the presence of both SAP and TSAP isomers, and because of several broad signals related to the relatively fast isomerization. In the temperature range of 273−353K, the ^{1}H NMR signals of Ln(DO3A−SA) complexes broaden with increasing temperature until 303 K, as expected for signals being in "slow exchange regime" (Figures S13−S15). The signals of the two isomers of the paramagnetic Eu(DO3A−SA) and the diamagnetic Y(DO3A−SA) and Lu(DO3A−SA) broaden and move closer to each other, and finally the two sets of signals coalesce at 303 K. The dynamic behaviors of Ln(DO3A−SA) complexes have been examined by ^{13}C NMR spectroscopy (Ln^{3+} = La^{3+}, Eu^{3+}, Y^{3+}, and Lu^{3+}). The variable temperature ^{13}C NMR spectra of La(DO3A−SA) complexes are shown in Figure 5, whereas those of Eu(DO3A−SA), Y(DO3A−SA), and Lu(DO3A−SA) are presented in Figures S18−S20, respectively. The ^{13}C NMR spectra of La(DO3A−SA) recorded at 273 and 353 K contain 16 and 12 signals, respectively. Because of the TSAP structure of La(DO3A−SA) complex, it can be assumed that the broadening and coalescence of signals is caused by the increased rate of enantiomerization. In the ^{13}C NMR spectra of La(DO3A−SA) obtained at 273 K, the *m*, *n*, and *l* carbon signals give rise virtually to two singlets, because the signals of the *m* and *n* carbons overlap. At 293 K, the signals of the *m* and *n* carbons are separated and three broad singlets are observed for the *m*, *n*, and *l* carbons. A further increase of temperature results in the coalescence of the *n* and *l* carbon signals, which can be explained by the fast enantiomerization of the TSAP isomers of La(DO3A−SA) (Scheme 2) on the actual NMR time scale. The ^{13}C NMR signals of the $-COO^{-}$ carbons (*l*, *m*, and *n*) are well-separated from the other signals, so it is possible to carry out line-shape analysis by simulating the ^{13}C NMR spectra obtained at different temperatures. Because the line widths of the *k* carbon signal do not change below 293 K, the transverse relaxation time (T_2) has been calculated from the *k* carbon

Scheme 2. Enantiomerization Process of the Λ(λλλλ) and Δ(δδδδ) Isomers of La(DO3A−SA)

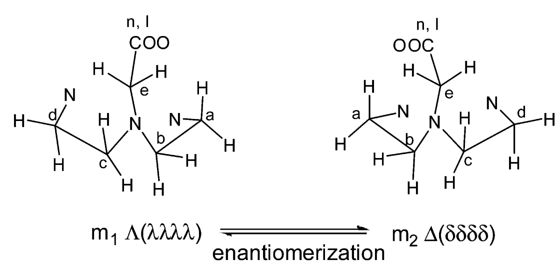

signal of La(DO3A−SA) obtained at 273 K (T_2 = 0.16 s). The experimental spectra have been simulated by the use of the chemical shift difference of the *l* and *n* carbon signals ($\Delta\delta$ = 74.4 Hz). Examples for typical experimental and simulated spectra are shown in Figure 6.

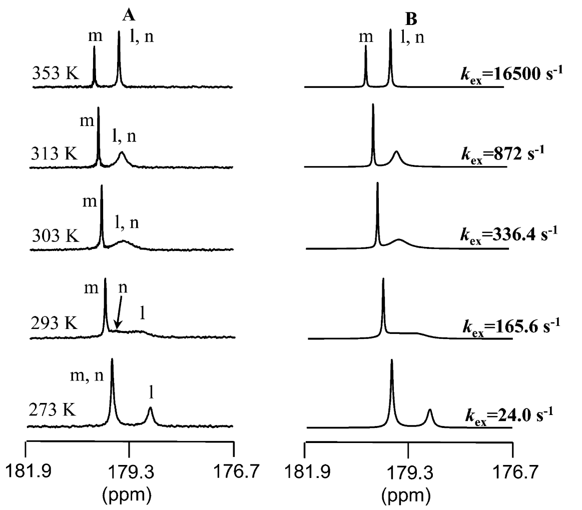

Figure 6. Experimental (A) and simulated (B) ^{13}C NMR signals of the *l*, *m*, and *n* carbon atoms of La(DO3A−SA).

The rate constants characterizing the exchange process (k_{ex} = $1/\tau$) have been calculated from the average conformation lifetimes (τ), which were obtained by the line-shape analysis with the use of the following equation

$$\frac{1}{*T_2} = \frac{1}{T_2} + \frac{1}{\tau} = \frac{T_2 + \tau}{T_2\tau} \quad (8)$$

where $*T_2$ is the transversal relaxation time of *l*, *m*, and *n* carbons at a given temperature. Line-shape analysis has also been performed on the *l*, *m*, and *n* carbon signals of Y(DO3A−SA) and Lu(DO3A−SA) complexes. Because of the presence of both SAP and TSAP isomers, the line-shape analysis of the *l*, *m*, and *n* carbon signals have been carried out at $T > 293$ K for Y(DO3A−SA) and Lu(DO3A−SA) complexes. The experimental and simulated ^{13}C NMR spectra of Y(DO3A−SA) and Lu(DO3A−SA) complexes are shown in Figures S21 and S22. The activation parameters of the isomerization processes obtained from the ^{13}C NMR studies of La(DO3A−SA), Y(DO3A−SA), and Lu(DO3A−SA) complexes (Table 5) have been estimated using the Eyring equation. The Eyring plots for the determination of the activation parameters for the arm rotation in La(DO3A−SA), Y(DO3A−SA), and Lu(DO3A−SA) complexes are shown in Figure S23.

Our band shape analysis provides very similar activation enthalpy ($\Delta H^{\ddagger}$) but quite different activation entropy ($\Delta S^{\ddagger}$), activation free energy ($\Delta G^{\ddagger}_{298}$), and exchange rate ($k_{ex}^{298}$) values for the isomerization processes of Ln(DO3A−SA) complexes. Generally, the $\Delta G^{\ddagger}$ and k_{ex} values for the arm rotation and the ring inversion processes of the Ln^{3+} complexes formed with DOTA-like chelates are relatively insensitive to the size of the encapsulated ion.[60,61,64,67,68] Comparison of the $\Delta G^{\ddagger}_{298}$ values presented in Table 5 indicates that the activation free energies of the isomerization processes of Y(DO3A−SA) and Lu(DO3A−SA) are similar and lower than that of La(DO3A−SA). By taking into account this observation, it can be assumed that the reaction pathway and rate-determining step of the isomerization of La(DO3A−SA) differs from those of Y(DO3A−SA) and Lu(DO3A−SA). Because the 100% of La(DO3A−SA) is present as TSAP, whereas about 7 and 93% of Y(DO3A−SA) and Lu(DO3A−SA) are present as TSAP and SAP isomers, the exchange process that leads to the broadening of *l* and *n* carbons is attributed to enantiomerization of TSAP isomers of La(DO3A−SA) and the SAP−TSAP interconversion of the Y(DO3A−SA) and Lu(DO3A−SA). The enantiomerization process of the La(DO3A−SA) requires the inversion of the cyclen ring ($\lambda\lambda\lambda\lambda \rightleftharpoons \delta\delta\delta\delta$) either before or after the rotation of the pendant arms ($\Lambda \rightleftharpoons \Delta$). However, the SAP−TSAP interconversion of Y(DO3A−SA) and Lu(DO3A−SA) can be realized by the arm rotation ($\Delta \rightleftharpoons \Lambda$) or by the ring inversion ($\lambda\lambda\lambda\lambda \rightleftharpoons \delta\delta\delta\delta$) processes. By considering the typical activation free energy of the cyclen inversion ($\Delta G^{\ddagger}_{298}$ = 55−65 kJ mol^{-1}),[67] it can be assumed that the SAP−TSAP interconversion of the Y(DO3A−SA) and Lu(DO3A−SA) takes place by the arm rotation as a rate-determining step characterized by 53 and 52 kJ mol^{-1} activation free energies ($\Delta G^{\ddagger}_{298}$), respectively. Because both the ring inversion and the arm rotation are required for the enantiomerization of TSAP isomers, the higher activation free energy value of La(DO3A−SA) ($\Delta G^{\ddagger}_{298}$ = 59 kJ mol^{-1}) obtained from the ^{13}C NMR studies is probably related to the activation barrier of the ring inversion, which is the rate-determining step of the enantimerization.

A comparison of the activation free energy obtained for the arm rotation process in Ln(DO3A−SA) complexes ($\Delta G^{\ddagger}_{298}$ = 53 and 52 for Y^{3+} and Lu^{3+}, respectively) with that obtained for Lu(DOTA) ($\Delta G^{\ddagger}_{298}$ = 65.3 kJ·mol^{-1})[60] indicates that the replacement of one acetate pendant arm of Ln(DOTA) with arylsulphonamide group decreases the rigidity of the coordination cage wrapping around the Ln^{3+} ion due to the larger flexibility of the ethylene group of the arylsulphonamide pendant.

DFT Geometry Optimization. Both 1D and 2D NMR studies of Ln(DO3A−SA) complexes provided a plethora of

Table 5. Rate Constants and Activation Parameters for the Isomerization Processes of Ln(DO3A−SA) (Ln = La, Y, and Lu) Complexes Obtained from the Line-Shape Analysis of the ^{13}C NMR Spectra[a]

	La(DO3A−SA)	Y(DO3A−SA)	Lu(DO3A−SA)
$\Delta H^{\ddagger}$ (kJ·mol^{-1})	62 ± 1	59 ± 3	60 ± 2
$\Delta S^{\ddagger}$ (J·mol^{-1} K^{-1})	12 ± 2	17 ± 2	27 ± 3
$\Delta G^{\ddagger}_{298}$ (kJ·mol^{-1})	59 ± 1	53 ± 1	52 ± 1
$\Delta G^{\ddagger}_{321}$ (kJ·mol^{-1})	58 ± 1	53 ± 1	51 ± 1
k_{ex}^{298} (s^{-1})	253 ± 3	(2.1 ± 0.2) × 10^3	(4.4 ± 0.4) × 10^3

[a]Eu(DO3A−SA): $\Delta G^{\ddagger}_{333}$ = 53 kJ·mol^{-1} (from the coalescence of the l and *n* carbon signals); Eu(DOTA): $\Delta G^{\ddagger}_{321}$ = 63.6 kJ·mol^{-1} (ref 61); Lu(DOTA): $\Delta G^{\ddagger}_{298}$ = 65.3 kJ·mol^{-1} (ref 60).

information about solution structure of our complexes. However, theoretical modeling is ultimately required to understand the relation between structure and function. Following the structural and dynamical study of Ln(DO3A−SA) complexes by means of NMR spectroscopy, we have decided to carry out computational modeling. The La(DO3A−SA), Eu(DO3A−SA), and Lu(DO3A−SA) complexes have been selected for geometry optimization calculations at the DFT level (B3LYP functional) focusing on conformational properties and energies of SAP and TSAP isomers, as well as the mechanism of the arm rotation processes.

It can be assumed that the solution structure of the protonated Ln(HDO3A−SA) highly resembles the corresponding Ln(DO3A) complexes with one or two water molecules directly coordinated to Ln^{3+} ion. According to our DFT calculation, the Ln(DO3A−SA) complexes are more stable if the SA group is coordinated to the metal ions with the replacement of the inner-sphere water molecule(s) (about 50−60 kJ/mol for the La^{3+} and about 60−80 kJ/mol for Lu^{3+} complexes). In this case, not only the nitrogen of the SA group but also one of the oxygen atoms of the sulphonamide group is coordinated, causing the substitution of the inner-sphere water molecule(s). Ln(DOTA)-like complexes usually have four possible stereoisomers, existing as two enantiomeric pairs which are different in the helicity of the pendant arms and macrocyclic ring.[62] Moreover, the coordination of the sulphonamide oxygens to the Ln^{3+} ion results in two isomers due to the presence of two sulphonamide oxygen atoms. By taking into account the SAP/TSAP diastereomers, eight different isomers are formed (four enantiomer pairs) where the SAP^R/SAP^L and $TSAP^R/TSAP^L$ diastereomers have different orientations of the benzene ring caused by the coordination of the two oxygen atoms of the SA group. (The relative position of the benzene ring is indicated by L (left) and R (right) in the superscript of the related isomers.) The SAP^R/SAP^L ($\Lambda(\delta\delta\delta\delta)$) and $TSAP^R/TSAP^L$ ($\Delta(\delta\delta\delta\delta)$) diastereomers of the eight possible isomers of Ln(DO3A−SA) are shown in Figure 7.

To obtain further information about the structural and dynamic behavior we have studied the interconversion processes among the isomers of La(DO3A−SA), Eu(DO3A−SA) and Lu(DO3A−SA) complexes. The calculated main structural parameters are summarized in Table S4. In vacuo calculations show a longer Ln−N distances compared to the X-ray data.[68] These differences can partially be ascribed to the fact that the large-core ECPs usually provide bond distances ca. 0.05−0.07 Å longer than the experimental ones.[69,70] Gaussian 03 PCM calculations had convergence problems[71−73] but PCM in Gaussian 09 with a new algorithm is more useful for geometry optimizations.[74] Therefore geometry optimizations were also carried out using PCM model of Gaussian 09 which shows a stronger interaction between metal ions and nitrogen atoms of the tetraaza ring of the ligand. It also means that the interactions with the oxygen atoms are relatively weaker, especially for the oxygen atom of the sulphonamide arm. This effect can be explained as a higher stabilization of the charges of the coordinated oxygen atoms, weakening the interaction between the central metal ion and the oxygen atoms of the carboxylate pendant arms. This can be seen via the parameters of $Ln-P_N$ and $Ln-P_{O-N}$ (Table S4) which are the distances between the metal ions and the plane of the four nitrogen atoms of the tetraaza ring and the four donor atoms of the pendant arms (the charged oxygen atoms of the three acetate

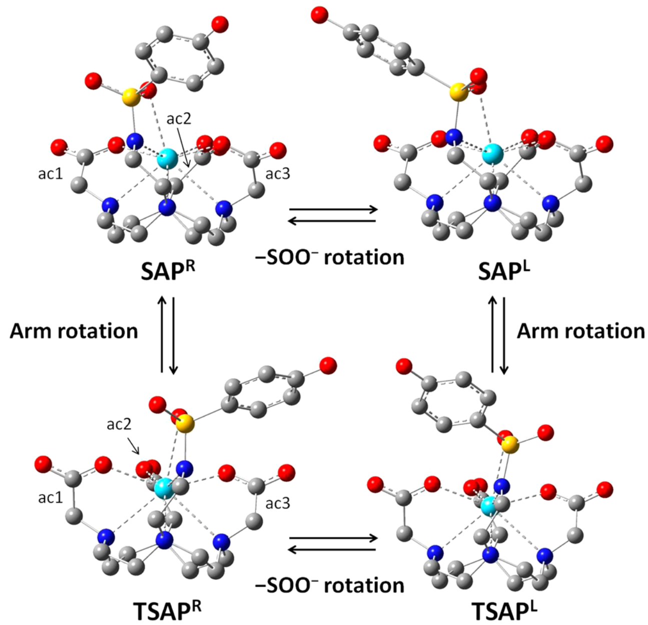

Figure 7. SAP^R/SAP^L ($\Lambda(\delta\delta\delta\delta)$) and $TSAP^R/TSAP^L$ ($\Delta(\delta\delta\delta\delta)$) diastereomers of the Ln(DO3A−SA) complexes. Acetate arms are labeled as ac1, ac2, and ac3.

groups and the nitrogen atom of the SA), respectively. By using PCM, the $Ln-P_{O-N}$ increases substantially while the $Ln-P_N$ decreases at the same time. For lanthanum, these changes are smaller: ∼0.1−0.15 Å for $La-P_{O-N}$, ∼0.15−0.2 Å for $La-P_N$, ∼0.15−0.2 Å for the $Ln-P_{O-N}$, and ∼0.2−0.25 Å for the $Ln-P_N$ in the cases of europium and lutecium, respectively. This means that the oxygen atom of the SA is getting much further from the metal ion in all cases (Table S4).

The Ln(DO3A−SA) complexes are distorted in all isomers. Most of the parameters are different for all of the pendant arms (Table S4). Only the twist angles (ω) of the ac1 and ac3 arms are similar. This is somewhat surprising, because the chemical environment of ac1 and ac3 arms is different. Twist angles of Ln(DOTA)-like complexes are larger in SAP isomers compared to TSAP, meaning that the P_{O-N} and P_N planes are located much farther from each other in the TSAP isomers. This is also valid for both in vacuo and PCM optimized structures.

Regarding the SAP^R/SAP^L and $TSAP^R/TSAP^L$ isomers, we have found that in vacuo the oxygen exchange of the sulphonamide group has a quite large activation barrier, which becomes much lower using PCM (Table 6). This is rational, because the bond length between the coordinated oxygen atom of the SA and the central ion is longer using PCM in all isomers, making the SA more labile. Otherwise, the transition state of the exchange processes could also be stabilized in the polarizable continuum. Because the NMR studies of Ln(DO3A−SA) complexes reveal that the oxygen

Table 6. Activation Barriers (Gibbs Free Energies) for the Oxygen Exchange Process of the Sulphonamide Group in Ln(DO3A−SA) Complexes

	La(DO3A−SA)		Eu(DO3A−SA)		Lu(DO3A−SA)	
rel energy (kJ/mol)	in vacuo	PCM	in vacuo	PCM	in vacuo	PCM
$TS_{SAP\text{-}SOO}$	78	22	74	30	68	30
$TS_{TSAP\text{-}SOO}$	83	24	74	28	58	25

exchange of the sulphonamide group is a fast process, it can be assumed that the results of the PCM calculations are reliable.

The relative population of the TSAP and SAP conformations of Ln(DO3A−SA) complex has been studied in detail by using NMR spectroscopy. The populations of the isomers can be easily derived from the calculated relative free energies using the formula $\Delta G° = -RT \ln K$. The relative population of the Ln(DO3A−SA) diastereomers obtained from DFT calculations is shown in Table 7.

Table 7. Populations of the TSAP Isomer of Ln(DO3A−SA) Complexes

TSAP %	in vacuo	PCM	exptl
La(DO3A−SA)	25	100	100
Eu(DO3A−SA)	9	97	15
Lu(DO3A−SA)	4	75	7

We could calculate relative energies for the different species without any convergence problem by using PCM. We have found that La(DO3A−SA) complex has only TSAP isomer in solution which is represented by PCM calculations. However, it has to be noted that PCM overrates the stabilization of the TSAP for Eu(DO3A−SA) and Lu(DO3A−SA) complexes (Table 7). Stabilization of the TSAP isomer with respect to the SAP by solvent effects has been previously observed for $[Ln(DOTA)(H_2O)]^-$ complexes.[75] This can be attributed to the different polarities of the two isomers: the TSAP isomer is more polar, and consequently, it is more stabilized by polar solvents.[75] However, the calculated tendency of the isomer population ratios along the lanthanide series is in agreement with the experimental data.

We have also made theoretical calculations to see the mechanism between SAP and TSAP isomers and make a comparison among Ln^{3+} ions with different sizes. For this, we have chosen lanthanum, europium, and lutetium complexes. The interconversion processes between the TSAP and SAP isomers takes place via two different pathways: (i) the inversion of the five-membered chelate rings of the tetra-aza ring of the macrocycle ligands, which leads to a $(\delta\delta\delta\delta) \leftrightarrow (\lambda\lambda\lambda\lambda)$ conformational change and (ii) the rotation of the pendant arms, which results in a $\Delta \leftrightarrow \Lambda$ configuration change.

In fact, only the pendant arm rotation has been investigated, because previous works state that this is the rate-determining step.[60,61,64,68] There are two reversible pathways for the $SAP^R \leftrightarrow TSAP^R$ interconversion and two reversible pathways for the $SAP^L \leftrightarrow TSAP^L$ interconversion of La(DO3A−SA), too. For Eu(DO3A−SA), there are two reversible pathways for the $SAP^R \leftrightarrow TSAP^R$ interconversion, though only one reversible pathway for the $SAP^L \leftrightarrow TSAP^L$ interconversion. For Lu(DO3A−SA), there is one reversible pathway for the $SAP^R \leftrightarrow TSAP^R$ interconversion and also one reversible pathway for $SAP^L \leftrightarrow TSAP^L$ interconversion, respectively. The number of possible interconversion pathways decreases with the lowering size of the Ln^{3+} ions, which inhibits the rotation of the sulphonamide pendant arm in the $TSAP^R$ and $TSAP^L$ isomers. Moreover, the position of the benzene ring has a steric hindrance for the rotation of the sulphonamide pendant arm in $TSAP^L$ isomer of Lu(DO3A−SA). In Figures 8 and 9 are shown the two reversible pathways of the $SAP^R \leftrightarrow TSAP^R$ interconversion of the La(DO3A−SA) complex obtained from in vacuo and PCM calculations, respectively. The transition

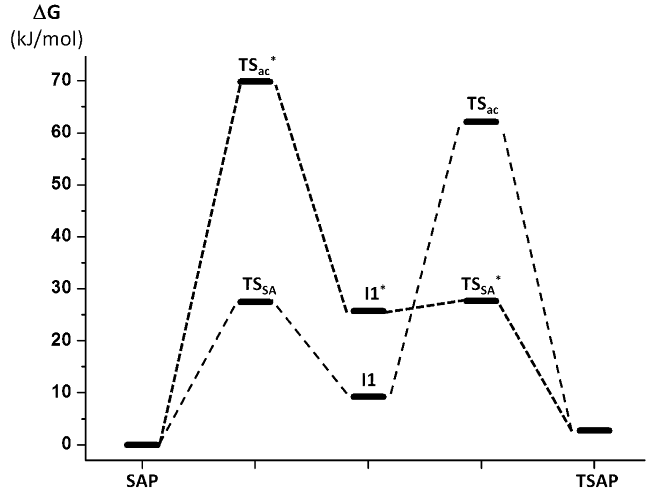

Figure 8. In vacuo energy profile of the $SAP^R \leftrightarrow TSAP^R$ interconversion of La(DO3A−SA) complex.

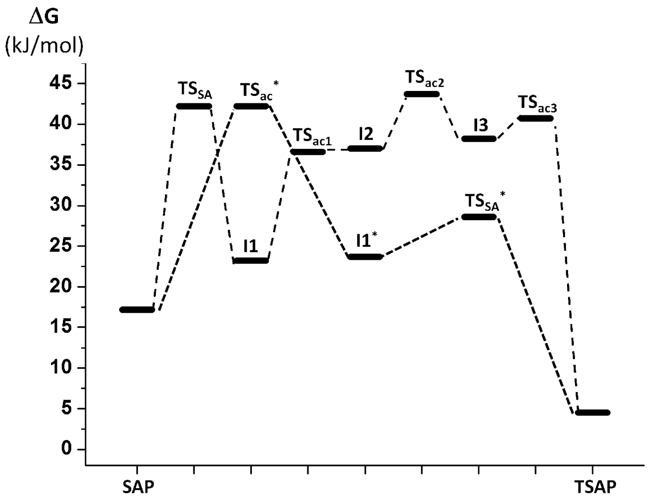

Figure 9. PCM energy profile of the $SAP^R \leftrightarrow TSAP^R$ interconversion of La(DO3A−SA) complex.

states and intermediates of the interconversion process are labeled by TS and I, respectively.

In vacuo calculations show that the three acetate groups are rotating together, separately from the sulphonamide (SA) group in all Ln(DO3A−SA) complexes. Energetically, the rotation of the SA is much more favorable than the acetate arm rotation, with the formation of a relative stable intermediate (I1). The activation energy of the rotation of the SA group is about half of the acetate rotation. This is in good agreement with the NMR studies.

The energy barriers decrease using PCM, and in some cases, the concerted acetate rotation is separated into individual conversion of ac1, ac2, and ac3. For lanthanum, the three acetate arms rotate independently from each other in the TSAP isomers, whereas the acetate arm rotation remains a concerted process starting from SAP isomer (Figure 9). A different process has been found only for the SAP isomer of the Eu(DO3A−SA) when comparing PCM and in vacuo calculations. In this case, two acetates turn together, followed by the rotation of the third acetate. The Gibbs free energies of the $SAP^R \leftrightarrow TSAP^R$ and $SAP^L \leftrightarrow TSAP^L$ interconversions processes are collected in Table S5. From the assigned values, we can calculate the energies of the rate-determining steps for the arm rotation processes of Ln(DO3A−SA) complexes. (The oxygen exchange of the sulphonamide group was not considered.) The energy values of the rate-determining step are compared with the experimental data in Table 8. From these data, it is apparent that the energy values obtained by theoretical calculations and by the NMR studies are similar. PCM calculations give energy values closer to the experimental results for Eu(DO3A−SA) and Lu(DO3A−SA), whereas the $\Delta G^{\ddagger}_{298}$ values obtained by PCM calculation and by the NMR experiment are in a good agreement for Eu(DO3A−SA). The result of the PCM calculations shows that the $\Delta G^{\ddagger}_{298}$ value of La(DO3A−SA) is lower than that of Eu(DO3A−SA) and Lu(DO3A−SA), which might be explained by the stabilization of the intermediates formed in the arm rotation processes of the lighter Ln(DO3A−SA) complexes. The activation free energy for the arm rotation process of La(DO3A−SA) obtained by PCM calculations is significantly lower than the typical $\Delta G^{\ddagger}_{298}$ values of the cyclen inversion process ($\Delta G^{\ddagger}_{298}$ = 55−65 kJ mol^{-1}),[67] which confirms that the rate-determining step of the enantiomerization is the ring inversion process of the La(DO3A−SA).

Table 8. Gibbs Free Energies ($\Delta G^{\ddagger}_{298}$) of the Rate-Determining Steps for the Arm Rotational Processes of Ln(DO3A−SA) Complexes

$\Delta G^{\ddagger}_{298}$ (kJ/mol)	in vacuo	PCM	NMR study
La(DO3A−SA)	65	36	
Eu(DO3A−SA)	61	49	54
Lu(DO3A−SA)	48	44	52

■ CONCLUSIONS

The complex Gd(DO3A−SA) is a promising pH-sensitive MRI contrast agent based on the deprotonation and coordination of the sulphonamide group. The recent equilibrium studies indicate that the protonation constant of the sulphonamide NH group of the Gd(DO3A−SA) is $\log K_{GdHL}$ = 6.16; thus, the pH-dependent processes occur in the pH range of 5.8−7.4. The relaxivity strongly changes in this range, because the deprotonated ligand is octadentate in contrast to the heptadentate protonated HDO3A−SA ligand. The stability of the Ln(DO3A−SA) complexes (the conditional stability constant) is significantly high near physiological conditions. In the complexes of divalent metal ions (Mg^{2+}, Ca^{2+}, Mn^{2+}, Zn^{2+}, and Cu^{2+}), the deprotonation of the noncoordinating sulphonamide NH group occurs in the pH range of 8.5−12.0, similarly to the free ligand. The stability constants of the ML complexes of the DO3A−SA and DO3A ligands formed with divalent metals are similar, whereas the $\log K_{LnL}$ values of the Ln(DO3A−SA) complexes are higher than those of the Ln(DO3A) complexes.

The formation reaction of Ln^{3+} complexes in the pH range of 3.5−6.0 is slow, with a pathway through the formation of *Ln(H_3DO3A−SA) intermediate, and assisted by the OH^- ions. The transmetalation reactions of Gd(HDO3A−SA) and Gd(DO3A) with Cu^{2+} are controlled by the proton-assisted dissociation of complexes. The half-lives of dissociation of Gd(HDO3A−SA) and Gd(DO3A) at pH = 7.4 are 5.600 and 210.000 h, respectively. The ^{1}H and ^{13}C NMR studies indicate rigid structure of the deprotonated Ln(DO3A−SA) complexes and the formation of square antiprismatic and twisted square antiprismatic isomers. DFT calculations show that the population of TSAP isomer is higher and that the sulphonamide group has a higher flexibility, the rate-determining step of the isomerization process being the rotation of the acetate arms. These results are in good agreement with the experimental findings.

■ ASSOCIATED CONTENT

Ⓢ Supporting Information

Experimental details for the characterization of thermodynamic and kinetic properties of the DO3A−SA and DO3A complexes of Mg^{2+}, Ca^{2+}, Mn^{2+}, Zn^{2+}, Cu^{2+}, and Ln^{3+} ions. The bond distance and angle data of Cu(H_2DO3A−SA) complex in the solid state. ^{1}H, ^{13}C, and 2D EXSY NMR spectra of Ln(DO3A−SA) complexes. The main structural parameters and the Gibbs free energies of the SAP^R ↔ TSAP^R and SAP^L ↔ TSAP^L interconversions of the Ln(DO3A−SA) complexes. This material is available free of charge via the Internet at http://pubs.acs.org.

■ AUTHOR INFORMATION

Corresponding Authors

*E-mail: mczsozso@yahoo.co.uk. Fax: +36 518-600. Tel.: +36 52-512-900/23209 (Z.B.).

*E-mail: silvio.aime@unito.it. Fax: +39-011-6706487. Tel.: +39-011-6706451 (S.A.).

Notes

The authors declare no competing financial interest.

■ ACKNOWLEDGMENTS

This research was supported by the European Union and the State of Hungary, co-financed by the European Social Fund in the framework of TÁMOP-4.2.4.A/ 2-11/1-2012-0001 "National Excellence Program" (grant no. A2-MZPD-12-0038) (Zs. B). The research was supported by the EU and cofinanced by the European Social Fund under the project ENVIKUT (TÁMOP-4.2.2.A-11/1/KONV-2012-0043) (I.T., E.B., A.B., A.T.). The author also acknowledge the support of the Hungarian Scientific Research Fund (OTKA K109029). This work was partially supported by the European Union and the European Social Fund through project Supercomputer, the national virtual lab (grant no. TAMOP-4.2.2.C-11/1/KONV-2012-0010) (MP). This research was performed within the framework of the EU COST Action TD1004 "Theragnostics Imaging and Therapy: An Action to Develop Novel Nanosized Systems for Imaging-Guided Drug Delivery" and the Italy-Hungary Intergovernmental S&T Cooperation Program (HU11MO2-TET_10-1-2011-0202). Financial support of Bracco Imaging S.p.A. is gratefully acknowledged. We thank Eliana Gianolio and István Bányai for assisting in the NMR experiments and the interpretation of the data.

■ REFERENCES

(1) Caravan, P.; Ellison, J. J.; McMurry, T. J.; Lauffer, R. B. *Chem. Rev.* **1999**, *99*, 2293.

(2) Brücher, E.; Tircsó, G.; Baranyai, Z.; Kovács, Z.; Sherry, A. D. In *The Chemistry of Contrast Agents in Medical Magnetic Resonance Imaging*; Merbach, A., Helm, L., Tóth, É., Eds.; John Wiley & Sons, Ltd: New York, 2013; pp 157.

(3) Woods, M.; Zhang, S.; Sherry, A. D. *Curr. Med. Chem.: Immunol., Endocr. Metab. Agents* **2004**, *4*, 349.

(4) Bonnet, C. S.; Tei, L.; Botta, M.; Tóth, É: In *The Chemistry of Contrast Agents in Medical Magnetic Resonance Imaging*; Merbach, A.,

Helm, L., Tóth, É., Eds.; John Wiley & Sons, Ltd: New York, 2013; pp 343.
(5) Kumar, K.; Chang, C. A.; Tweedle, M. F. *Inorg. Chem.* **1993**, *32*, 587.
(6) Raghunand, N.; Zhang, S.; Sherry, A. D.; Gillies, R. J. *Acad. Radiol.* **2002**, *9*, S481.
(7) Raghunand, N.; Howison, C.; Sherry, A. D.; Zhang, S.; Gillies, R. J. *Magn. Reson. Med.* **2003**, *49*, 249.
(8) Garcia-Martin, M. L.; Martinez, G. V.; Raghunand, N.; Sherry, A. D.; Zhang, S.; Gillies, R. J. *Magn. Reson. Med.* **2006**, *55*, 309.
(9) De Leon-Rodriguez, L. M.; Lubag, A. J. M.; Malloy, C. R.; Martinez, G. V.; Gillies, R. J.; Sherry, A. D. *Acc. Chem. Res.* **2009**, *42*, 948.
(10) Martinez, G. V.; Zhang, X.; García-Martín, M. L.; Morse, D. L.; Woods, M.; Sherry, A. D.; Gillies, R. J. *NMR Biomed.* **2011**, *24*, 1380.
(11) Lowe, M. P.; Parker, D.; Reany, O.; Aime, S.; Botta, M.; Castellano, G.; Gianolio, E.; Pagliarin, R. *J. Am. Chem. Soc.* **2001**, *123*, 7601.
(12) Giovenzana, G. B.; Negri, R.; Rolla, G. A.; Tei, L. *Eur. J. Inorg. Chem.* **2012**, *2012*, 2035.
(13) Baranyai, Z.; Rolla, G. A.; Negri, R.; Forgács, A.; Giovenzana, G. B.; Tei, L. *Chem.—Eur. J.* **2014**, DOI: 10.1002/chem.201304063.
(14) Kumar, K.; Chang, C. A.; Francesconi, L. C.; Dischino, D. D.; Malley, M. F.; Gougoutas, J. Z.; Tweedle, M. F. *Inorg. Chem.* **1994**, *33*, 3567.
(15) Koike, T.; Kimura, E.; Nakamura, I.; Hashimoto, Y.; Shiro, M. *J. Am. Chem. Soc.* **1992**, *114*, 7338.
(16) Lowe, M. P.; Parker, D. *Chem. Commun.* **2000**, 707.
(17) Gianolio, E.; Napolitano, R.; Fedeli, F.; Arena, F.; Aime, S. *Chem. Commun.* **2009**, 6044.
(18) Frullano, L.; Catana, C.; Benner, T.; Sherry, A. D.; Caravan, P. *Angew. Chem., Int. Ed.* **2010**, *49*, 2382.
(19) Gianolio, E.; Maciocco, L.; Imperio, D.; Giovenzana, G. B.; Simonelli, F.; Abbas, K.; Bisi, G.; Aime, S. *Chem. Commun.* **2011**, *47*, 1539.
(20) Irving, H. M.; Miles, M. G.; Pettit, L. D. *Anal. Chim. Acta* **1967**, *38*, 475.
(21) Zekany, L.; Nagypal, I. In *Computational Methods for the Determination of Formation Constants*; Leget, D. J., Ed.; Plenum Press: New York, 1985, p 291.
(22) Kasprzyk, S. P.; Wilkins, R. G. *Inorg. Chem.* **1982**, *21*, 3349.
(23) Becke, A. D. *J. Chem. Phys.* **1993**, *98*, 5648.
(24) Lee, C.; Yang, W.; Parr, R. G. *Phys. Rev. B* **1988**, *37*, 785.
(25) Frisch, M. J.; Trucks, G. W.; Schlegel, H. B.; Scuseria, G. E.; Robb, M. A.; Cheeseman, J. R.; Scalmani, G.; Barone, V.; Mennucci, B.; Petersson, G. A.; Nakatsuji, H.; Caricato, M.; Li, X.; Hratchian, H. P.; Izmaylov, A. F.; Bloino, J.; Zheng, G.; Sonnenberg, J. L.; Hada, M.; Ehara, M.; Toyota, K.; Fukuda, R.; Hasegawa, J.; Ishida, M.; Nakajima, T.; Honda, Y.; Kitao, O.; Nakai, H.; Vreven, T.; Montgomery, J. A.; Peralta, J. E.; Ogliaro, F.; Bearpark, M.; Heyd, J. J.; Brothers, E.; Kudin, K. N.; Staroverov, V. N.; Kobayashi, R.; Normand, J.; Raghavachari, K.; Rendell, A.; Burant, J. C.; Iyengar, S. S.; Tomasi, J.; Cossi, M.; Rega, N.; Millam, J. M.; Klene, M.; Knox, J. E.; Cross, J. B.; Bakken, V.; Adamo, C.; Jaramillo, J.; Gomperts, R.; Stratmann, R. E.; Yazyev, O.; Austin, A. J.; Cammi, R.; Pomelli, C.; Ochterski, J. W.; Martin, R. L.; Morokuma, K.; Zakrzewski, V. G.; Voth, G. A.; Salvador, P.; Dannenberg, J. J.; Dapprich, S.; Daniels, A. D.; Farkas; Foresman, J. B.; Ortiz, J. V.; Cioslowski, J.; Fox, D. J.*Gaussian 09*; Gaussian, Inc.: Wallingford, CT, 2009.
(26) Tomasi, J.; Mennucci, B.; Cammi, R. *Chem. Rev.* **2005**, *105*, 2999.
(27) Scalmani, G.; Frisch, M. J. *J. Chem. Phys.* **2010**, *132*, 114110.
(28) Maron, L.; Eisenstein, O. *J. Phys. Chem. A* **2000**, *104*, 7140.
(29) Boehme, C.; Coupez, B.; Wipff, G. *J. Phys. Chem. A* **2002**, *106*, 6487.
(30) Ingram, K. I. M.; Tassell, M. J.; Gaunt, A. J.; Kaltsoyannis, N. *Inorg. Chem.* **2008**, *47*, 7824.
(31) Dolg, M.; Stoll, H.; Preuss, H. *J. Chem. Phys.* **1989**, *90*, 1730.
(32) Harms, K.; Wocadlo, S. University of Marburg, Marburg, Germany, 1995.
(33) Altomare, A.; Cascarano, G.; Giacovazzo, C.; Guagliardi, A. *J. Appl. Crystallogr.* **1993**, *26*, 343.
(34) Sheldrick, G. M. *Acta Crystallogr., Sect. A* **2008**, *64*, 112.
(35) Spek, A. *J. Appl. Crystallogr.* **2003**, *36*, 7.
(36) Farrugia, L. *J. Appl. Crystallogr.* **1999**, *32*, 837.
(37) Martell, A. E.; Smith, R. M. *Critical Stability Constants*; Plenum Press: New York, 1974−1982; Vol. *1*−*5*.
(38) Delgado, R.; da Silva, J. J. R. F.; Vaz, M. C. T. A.; Paoletti, P.; Micheloni, M. *J. Chem. Soc., Dalton Trans.* **1989**, 133.
(39) Cai, H.-Z.; Kaden, T. A. *Helv. Chim. Acta* **1994**, *77*, 383.
(40) Tircso, G.; Woods, M.; Nagy, N.; Baranyai, Z. 2014, to be published.
(41) Lowe, M. P.; Parker, D. *Inorg. Chim. Acta* **2001**, *317*, 163.
(42) Cacheris, W. P.; Nickle, S. K.; Sherry, A. D. *Inorg. Chem.* **1987**, *26*, 958.
(43) Kumar, K.; Tweedle, M. F.; Malley, M. F.; Gougoutas, J. Z. *Inorg. Chem.* **1995**, *34*, 6472.
(44) Riesen, A.; Zehnder, M.; Kaden, T. A. *Helv. Chim. Acta* **1986**, *69*, 2067.
(45) Toth, E.; Brucher, E.; Lazar, I.; Toth, I. *Inorg. Chem.* **1994**, *33*, 4070.
(46) Brücher, E.; Laurenczy, G.; Makra, Z. S. *Inorg. Chim. Acta* **1987**, *139*, 141.
(47) Wang, X.; Jin, T.; Comblin, V.; Lopez-Mut, A.; Merciny, E.; Desreux, J. F. *Inorg. Chem.* **1992**, *31*, 1095.
(48) Wu, S. L.; Horrocks, W. D. *Inorg. Chem.* **1995**, *34*, 3724.
(49) Moreau, J.; Guillon, E.; Pierrard, J. C.; Rimbault, J.; Port, M.; Aplincourt, M. *Chem.—Eur. J.* **2004**, *10*, 5218.
(50) Burai, L.; Fabian, I.; Kiraly, R.; Szilagyi, E.; Brucher, E. *J. Chem. Soc., Dalton Trans.* **1998**, 243.
(51) Brucher, E.; Sherry, A. D. *Inorg. Chem.* **1990**, *29*, 1555.
(52) Kumar, K.; Tweedle, M. F. *Inorg. Chem.* **1993**, *32*, 4193.
(53) Szilágyi, E.; Tóth, É.; Kovács, Z.; Platzek, J.; Radüchel, B.; Brücher, E. *Inorg. Chim. Acta* **2000**, *298*, 226.
(54) Baranyai, Z.; Palinkas, Z.; Uggeri, F.; Maiocchi, A.; Aime, S.; Brucher, E. *Chem.—Eur. J.* **2012**, *18*, 16426.
(55) Toth, E.; Kiraly, R.; Platzek, J.; Raduchel, B.; Brucher, E. *Inorg. Chim. Acta* **1996**, *249*, 191.
(56) Kumar, K.; Jin, T.; Wang, X.; Desreux, J. F.; Tweedle, M. F. *Inorg. Chem.* **1994**, *33*, 3823.
(57) Spirlet, M. R.; Rebizant, J.; Loncin, M. F.; Desreux, J. F. *Inorg. Chem.* **1984**, *23*, 4278.
(58) Chang, C. A.; Francesconi, L. C.; Malley, M. F.; Kumar, K.; Gougoutas, J. Z.; Tweedle, M. F.; Lee, D. W.; Wilson, L. J. *Inorg. Chem.* **1993**, *32*, 3501.
(59) Parker, D.; Pulukkody, K.; Smith, F. C.; Batsanov, A.; Howard, J. A. K. *J. Chem. Soc., Dalton Trans.* **1994**, 689.
(60) Aime, S.; Barge, A.; Botta, M.; Fasano, M.; Danilo Ayala, J.; Bombieri, G. *Inorg. Chim. Acta* **1996**, *246*, 423.
(61) Desreux, J. F. *Inorg. Chem.* **1980**, *19*, 1319.
(62) Aime, S.; Botta, M.; Ermondi, G. *Inorg. Chem.* **1992**, *31*, 4291.
(63) Hoeft, S.; Roth, K. *Chem. Ber.* **1993**, *126*, 869.
(64) Jacques, V.; Desreux, J. F. *Inorg. Chem.* **1994**, *33*, 4048.
(65) Aime, S.; Botta, M.; Fasano, M.; Marques, M. P. M.; Geraldes, C. F. G. C.; Pubanz, D.; Merbach, A. E. *Inorg. Chem.* **1997**, *36*, 2059.
(66) Aoki, S.; Kawatani, H.; Goto, T.; Kimura, E.; Shiro, M. *J. Am. Chem. Soc.* **2001**, *123*, 1123.
(67) Platas-Iglesias, C. *Eur. J. Inorg. Chem.* **2012**, *2012*, 2023.
(68) Purgel, M. L.; Baranyai, Z.; de Blas, A. S.; Rodríguez-Blas, T.; Bányai, I. N.; Platas-Iglesias, C.; Tóth, I. *Inorg. Chem.* **2010**, *49*, 4370.
(69) Heiberg, H.; Gropen, O.; Laerdahl, J. K.; Swang, O.; Wahlgren, U. *Theor. Chem. Acc.* **2003**, *110*, 118.
(70) Buzko, V.; Sukhno, I.; Buzko, M. *J. Mol. Struct.: THEOCHEM* **2009**, *894*, 75.
(71) Tsushima, S.; Yang, T.; Mochizuki, Y.; Okamoto, Y. *Chem. Phys. Lett.* **2003**, *375*, 204.
(72) Li, H.; Jensen, J. H. *J. Comput. Chem.* **2004**, *25*, 1449.

(73) Cosentino, U.; Pitea, D.; Moro, G.; Barone, V.; Villa, A.; Muller, R. N.; Botteman, F. *Theor. Chem. Acc.* **2004**, *111*, 204.
(74) Gausian 09 User's Reference: Changes Between Gaussian 09 and Gaussian 03. http://www.gaussian.com/g_tech/g_ur/a_gdiffs09.htm.
(75) Cosentino, U.; Villa, A.; Pitea, D.; Moro, G.; Barone, V.; Maiocchi, A. *J. Am. Chem. Soc.* **2002**, *124*, 4901.